EUROPEAN ORGANIZATION FOR NUCLEAR RESEARCH

CERN-EP/81-159
27.11.81

A STUDY OF INCLUSIVE PHOTOPRODUCTION OF HYPERONS AND ANTIHYPERONS IN THE RANGE OF 20 TO 70 GeV

Bonn[1]-CERN[2]-Ecole Polytechnique[3]-Glasgow[4]-Lancaster[5]-Manchester[6]-Orsay[7]-Paris VI[8]-Paris VII[9]-Rutherford[10]-Sheffield[11] Collaboration

D. Aston[10], M. Atkinson[10], R. Bailey[11], A.H. Ball[6], H.J. Bautsch[1], B. Bouquet[7], G.R. Brookes[11], J. Bröring[1], P.J. Bussey[4], D. Clarke[10], A.B. Clegg[5], B. D'Almagne[7], G. de Rosny[3], B. Diekmann[1], A. Donnachie[6], M. Draper[4], B. Drevillon[3], I.P. Duerdoth[6], J.-P. Dufey[2], R.J. Ellison[6], D. Ezra[6], P. Feller[1], A. Ferrer[7], P.J. Flynn[5], W. Galbraith[11], R. George[8], S.D.M. Gill[6], M. Goldberg[8], S. Goodman[8], W. Graves[3], B. Grossetête[9], P.G. Hampson[6], K. Heinloth[1], R.E. Hughes-Jones[6], J.S. Hutton[10], M. Ibbotson[6], M. Jung[1], S. Katsanevas[3], M.A.R. Kemp[10], F. Kovacs[9], B.R. Kumar[10], G.D. Lafferty[5], J.B. Lane[6], J.-M. Lévy[8], V. Liebenau[1], J. Litt[10], G. London[8], D. Mercer[6], J.V. Morris[10], K. Müller[1], D. Newton[5], E. Paul[1], P. Petroff[7], Y. Pons[9], C. Raine[11], F. Richard[7], R. Richter[1], J.H.C. Roberts[6], P. Roudeau[7], A. Rougé[3], M. Rumpf[3], M. Sené[8], J. Six[7], I.O. Skillicorn[4], J.C. Sleeman[4], K.M. Smith[4], C. Steinhauer[1], K.M. Storr[5], R.J. Thompson[6], D. Treille[2], Ch. de la Vaissière[8], H. Videau[3], I. Videau[3], A.P. Waite[6], A. Wijangco[3], W. Wojcik[7], J.-P. Wuthrick[3] and T.P. Yiou[8]

(Submitted to Nuclear Physics B)

ABSTRACT

Results are presented on inclusive photoproduction in hydrogen of Σ^0, $\Sigma^{\pm}_{1385}$, Ξ^0, and their antiparticles for incident energies between 20 and 70 GeV. Hyperons and antihyperons are mainly measured in the kinematical range of central and forward production ($x_F > -0.3$). We find the cross-section ratios $\sigma(\Sigma^+_{1385})/\sigma(\Sigma^-_{1385}) = 1.4 \pm 0.1$, $\sigma(\overline{\Sigma^+_{1385}})/\sigma(\overline{\Sigma^-_{1385}}) = 1.3 \pm 0.2$ and an antiparticle/particle ratio of about 0.3 for the three sigma states. The results suggest an important role of the valence quarks of both the beam projectile and target in the production process in qualitative agreement with current ideas of quark fusion models. The inclusive production of $\Sigma^{\pm}_{1385}$ is also observed in a small subsample of the events containing $\Lambda\bar{\Lambda}$ pairs. The x_F distribution of $\Lambda(\bar{\Lambda})$ in $\Lambda\bar{\Lambda}$ events as well as those in $\Lambda\bar{p}$ ($p\bar{\Lambda}$) is the same as those in single Λ ($\bar{\Lambda}$) inclusive events. Weak signals in the $K^-p\pi^+$ and $\Lambda\pi^+\pi^+\pi^-$ mass spectra are observed around a mass of 2.26 GeV.

1. INTRODUCTION

In this paper we present results of a study of inclusive production of strange baryons in photon proton interactions at photon energies from 20 to 70 GeV. The data originate from a general study of photoproduction of multiparticle final states carried out at the CERN SPS using the Omega spectrometer with a tagged photon beam.

The main part of this paper is concerned with Σ^0, $\Sigma^{\pm}_{1385}$, and Ξ^{0} and their antiparticles. The study of inclusive production of Λ and $\bar{\Lambda}$ based on the same data has been published separately[1]. The reactions investigated are listed in Table 1. No Ω^- signal has been observed. The kinematical range of x_F ($= 2p^*_{\parallel}/\sqrt{s}$) of the hyperon states accessible in this experiment is typically $x_F > -0.3$. The results are discussed in terms of a simple quark model picture by looking at cross-section ratios of charged hyperon states. Data of inclusive strange baryon production in the low mass range (baryon mass < 2.0 GeV) already exist from hadron-hadron collisions at high energies with incident pions[2,3], kaons[4,5], protons[6,7], and antiprotons[8].

The channels $K^-p\pi^{\pm}$ and $\Lambda(3\pi)^{\pm}$ are studied for baryons of mass > 2 GeV, and show some evidence for a signal at 2.26 GeV.

We report also on results of inclusive hyperon production in events with $\Lambda\bar{\Lambda}$, $\Lambda\bar{p}$ and $\bar{\Lambda}p$ pairs.

2. EXPERIMENT AND DATA

The layout of the experiment is shown in Fig. 1. The experimental details have been discussed elsewhere[9]. The features of the high multiplicity trigger conditions relevant for these data are given in Ref. 1. A Cerenkov counter was used to identify charged particles, giving light for pions with momenta $\geq$ 5.6 GeV, kaons with $\geq$ 18 GeV and protons with $\geq$ 34 GeV. It did not distinguish between a $K^+(K^-)$ and $p(\bar{p})$ in the range from 5.6 to 18 GeV. The fraction of protons in the K^+ sample was estimated to be 34 ± 4%, and for $\bar{p}$ in the K^- sample to be about 5%[10]. A photon detector measured photons in the momentum range of 0.5 to 20 GeV, and in a forward angular range of ±120 mrad[9].

We use the events from a trigger requiring a charge multiplicity ≥ 4 as described in Ref. 1. In addition to this trigger we add events from another trigger with the same multiplicity requirement plus at least one charged particle with no light in the Cerenkov counter, i.e. a koan or proton (antiproton). The effective sensitivity of our experiment for the reactions considered is in the order of $\sim 40\ nb^{-1}$.

3. SELECTION OF EVENTS

The selection of events containing a Λ or $\bar{\Lambda}$ is discussed in Ref. 1. The x_F range of $\Lambda(\bar{\Lambda})$ is restricted to $x_F > -0.3$ by the acceptance. Tracks with a momentum < 100 MeV either from a V^0 or from the main vertex were rejected because the acceptance for those tracks is not known sufficiently well. About 70% of the $\Lambda(\bar{\Lambda})$ could be unambiguously identified by detecting a $p(\bar{p})$ from their decays in the Cerenkov counter. The ambiguities between Λ/K^0_S and $\bar{\Lambda}/K^0_S$ were resolved by calculating the number of K^0_S in the ambiguous $\Lambda(\bar{\Lambda})$ sample from those mass distributions obtained by assuming the π mass for both decay particles. From this we estimated that 62% of the Λ/K^0_S ambiguities are in fact Λ, and 32% of $\bar{\Lambda}^0/K^0_S$ ambiguities are $\bar{\Lambda}$. Consequently, we weighted events with an ambiguous Λ by 0.62, and with an ambiguous $\bar{\Lambda}$ by 0.32. Using these weights and the acceptance for $\Lambda(\bar{\Lambda})$ (see Section 4), one finds a flat decay angular distribution in the helicity rest frame of the $\Lambda(\bar{\Lambda})$, as shown in Fig. 2. Figures 2a and 2b show, respectively, the cos θ distribution for the proton from the Λ, and for the π^+ from the $\bar{\Lambda}$ decays in the helicity frame of the V^0. The acceptance is indicated by the solid curve. The shaded areas give the contributions from the ambiguous cases. The final data sample includes $\sim$ 15000 Λ, $\sim$ 5000 $\bar{\Lambda}$ and $\sim$ 100 $\Lambda\bar{\Lambda}$.

In order to select events containing a proton and a K^-, we took events with at least one positively and one negatively charged particle with momentum above the π threshold and no light in the Cerenkov counter. This required restricting the photon energy to the range 40 to 70 GeV. We obtained a final sample of $\sim$ 26000 events with a proton and a K^-.

4. ACCEPTANCE

The acceptance of the hyperons in reactions (1) to (5) (see Table 1) was calculated by assuming a flat x_F distribution, a p_T^2 dependence of $e^{-3p_T^2}$, and isotropic angular distributions for the hyperon decays. The acceptance of Λ and $\bar{\Lambda}$ was taken from Ref. 1. The acceptance of the hyperons is virtually independent of p_T^2, as already found for Λ and $\bar{\Lambda}$. In Fig. 6a the acceptance for Σ^+_{1385} is shown as a function of x_F. This acceptance is the same for Σ^+_{1385}, Σ^-_{1385} and their antiparticles. For reactions (1) and (4), which contain a single photon or a π^0 in the final state, the acceptance of the photon detector limits the observed range of these hyperons to $x_F > 0.15$.

To calculate the acceptance for $\Xi^-(\overline{\Xi^-})$ we used the assumptions above. However, one has to consider a double decay, i.e.

$$\gamma p \rightarrow \Xi^- + X$$
$$\Xi^- \rightarrow \Lambda \pi_1^-$$
$$\Lambda \rightarrow p \pi_2^- \ .$$

Two samples of Ξ^- decays can be observed. In the first sample, the Ξ^- decays such that the π_1^- is attached to the main production vertex, due to the uncertainty of the vertex measurement, and therefore contains mainly short range decays. In the second sample the π_1^- is taken by the reconstruction program as an extra track due to long range decays of the Ξ^-. The first sample represents $\sim$ 70% and the second $\sim$ 30% of all Ξ^- decays. To calculate the cross section for Ξ^-, we used the events of both samples. In the case of the $\overline{\Xi^-}$, we used only the events of the first sample because of the limited statistics, and corrected for the losses due to the second sample.

In the case of the $\Xi^0(\overline{\Xi^0})$, which was studied by the corresponding double decay process ($\Xi^0 \rightarrow \Lambda\pi^0$) the problem arises that the direction of the π^0 (measured in the photon detector) was calculated by using the main vertex position as reference point. Thus for long range decays of the Ξ^0, the π^0 direction is distorted resulting in a worse mass resolution. The various effects on the acceptance have been studied by simulations with the assumptions already made for Ξ^-.

For reactions (9) and (10) the geometrical acceptance of the Cerenkov counter restricts the x_F range of the identified protons and kaons to $x_F > 0$.

Although the acceptance for all decay channels is known to only ±30%, the various losses cancel to first approximation when ratios of cross sections for inclusive hyperon or antihyperon production are considered.

5. PRODUCTION OF LOW MASS HYPERONS (BARYON MASS < 2 GeV)

5.1 Experimental results

A. Analysis of Σ states

In this section we report on the production of sigma states, i.e. Σ^0_{1132}, $\Sigma^{\pm}_{1385}$ and their antiparticles. Figure 3 shows the raw data mass distribution for $\Lambda\gamma$ (a) and $\bar{\Lambda}\gamma$ (b). There is clear evidence for signals at the nominal Σ^0 mass value, with a spread consistent with the experimental resolution. The numbers of Σ^0 and $\overline{\Sigma^0}$ were determined by fitting to the mass spectrum a Breit-Wigner resonance term (BW) and a background term (BG):

$$\frac{d\sigma}{dm} = a\ BG + b\ BW\ .$$

Here the Breit-Wigner function was taken to be of the form:

$$BW(m) = \frac{mm_R\Gamma}{(m^2 - m_R^2)^2 + m_R^2\Gamma^2}$$

where m_R is the resonance mass, taken as a free parameter. The width Γ was fixed for $\Sigma^0(\overline{\Sigma^0})$ to $\Gamma = 0.015$ GeV, consistent with the experimental resolution. To describe the background, a third-order polynomial was used. From the resulting fit, we get $m_R = 1.193 \pm 0.002$ GeV with a $\chi^2/NDF \approx 0.9$. We observe 250 ± 40 Σ^0 and 90 ± 25 $\overline{\Sigma^0}$ decays. Compared with the number of observed $\Lambda(\bar{\Lambda})$, the sample of observed $\Sigma^0(\overline{\Sigma^0})$ decays is small, because most of the photons originating from such decays do not hit the photon detector or have a momentum less than 500 MeV and cannot be measured by this detector (see Section 2). Accordingly, we give only the ratio $\sigma(\overline{\Sigma^0})/\sigma(\Sigma^0)$, assuming that the acceptance effects approximately cancel. This ratio is found to be 0.36 ± 0.1 (see Table 3) and constant over x_F ($x_F > 0.15$), within large errors.

The mass combinations $\Lambda\pi^+$ and $\Lambda\pi^-$ are shown in Fig. 4a and b, respectively, whilst those for $\bar{\Lambda}\pi^-$ and $\bar{\Lambda}\pi^+$ appear in Fig. 5a and b. To fit these mass distributions, the Breit-Wigner width Γ for the $\Sigma^{\pm}_{1385}$ signals was given the mass dependent form

$$\Gamma(m) = \Gamma_R (q/q_R)^{2\ell+1} \rho(m)/\rho(m_R)$$

where

$$\rho(m) = (q_R^2 + q^2)^{-1}$$

q being the momentum of each of the decay products in the resonance rest frame, q_R the value of q at the resonance mass and ℓ the relative angular momentum of the decay particles. The mass spectrum was fitted in the form

$$\frac{d\sigma}{dm} = BG(a + b\ BW)$$

with

$$BG(m) = \alpha(m - m_{Th})^{\beta}\ e^{-\gamma m}$$

where α, β and γ are determined by the fit and m_{Th} is the threshold mass for $\Lambda\pi$ combinations. This ansatz for parametrizing the background describes in all cases a mass distribution obtained by combining a $\Lambda(\bar{\Lambda})$ from one event in the data sample with the corresponding particle (π) found in a successive event of the same type. In all fits the width Γ_R of the $\Sigma^{\pm}_{1385}$ signals was fixed to $\Gamma_R = 0.045$ GeV, representing the natural width of $\Sigma_{1385} \sim 37$ MeV and the experimental resolution which is estimated to be in the range from 15 to 30 MeV. The fitted resonance masses do not vary significantly from the nominal value of $m_{\Sigma_{1385}} = 1.385$ GeV and the χ^2/NDF was found to be ~ 1 in all fits. The number of combinations in the peaks and the resulting cross sections are given in Table 2.

In the mass distribution of $\Lambda\pi^+$ combinations, as shown in Fig. 4a, a second enhancement is seen around 1.6 GeV, which has been included into the fit by an additional Breit-Wigner term. The uncertainty in the number of Σ^+_{1385} as given in Table 2, is estimated by a second fit in which the additional Breit-Wigner function has been omitted (not shown).

Figures 6 and 7 show the x_F distributions for Σ^+_{1385} and Σ^-_{1385} and their corresponding antiparticles. The number of $\Sigma^+_{1385}(\Sigma^-_{1385})$ as a function of x_F were obtained by fitting the mass spectra for each bin of x_F separately. The data are corrected for acceptance which is the same for Σ_{1385} and $\bar{\Sigma}_{1385}$.

The p_T^2 distributions for Σ^+_{1385} and Σ^-_{1385} and their antiparticles are shown in Figs. 8 and 9. The numbers of $\Sigma_{1385}(\bar{\Sigma}_{1385})$ as a function of p_T^2 are determined in the same way as described for the x_F distributions. The p_T^2 distributions for Σ_{1385} and $\bar{\Sigma}_{1385}$ were fitted by a function of the form

$$\frac{d\sigma}{dp_T^2} = a\ e^{-bp_T^2}$$

giving a value for the slope b for each hyperon as follows:

	$0 < p_T^2 < 1.2$ GeV^2		$0 < p_T^2 < 0.8$ GeV^2
Σ^+_{1385} :	$b = 2.6 \pm 0.2$ GeV^{-2}	$\overline{\Sigma^+_{1385}}$:	$b = 2.5 \pm 0.5$ GeV^{-2}
Σ^-_{1385} :	$b = 2.6 \pm 0.2$ GeV^{-2}	$\overline{\Sigma^-_{1385}}$:	$b = 3.0 \pm 0.7$ GeV^{-2}

B. Analysis of Ξ states

Figure 4b shows besides the Σ^-_{1385} also a small signal in the Ξ^- mass region. The Ξ^- was fitted by adding incoherently a second Breit-Wigner term with a variable resonance mass and a fixed width of 0.015 GeV as defined by the experimental resolution. The resonance mass was determined by the fit to be $m_R = 1.32 \pm 0.04$ GeV. The curve in Fig. 4b represents an overall fit including both resonances and the background term. In Table 2 we give the number of observed Ξ^- decays and the estimated cross section. Figure 4b contains the events of the first sample with a π^-_1 attached to the main vertex (see Section 4), whereas in Table 2 we include also the number of Ξ^- found in events from the second sample.

We fitted the data of Fig. 5b using the same procedure as above, including the $\overline{\Sigma^-_{1385}}$ and a contribution from $\overline{\Xi^-}$, by fixing the mass and the width of the latter at the values $m_R = 1.32$ GeV and $\Gamma = 0.015$ GeV. We observe 48 ± 15 events for the $\overline{\Xi^-}$.

The raw mass distributions of $\Lambda\pi^0$ and $\bar{\Lambda}\pi^0$ are shown in Figs. 10a and 10b. Due to the acceptance for π^0 (see Section 4) the x_F range of the $\Lambda\pi^0(\bar{\Lambda}\pi^0)$ system is limited to $x_F > 0.15$. Small signals in the $\Xi^0(\bar{\Xi}^0)$ mass region can be observed. Since the background cannot be estimated sufficiently well, no cross sections are given.

5.2 Discussion

It has been observed in inclusive photoproduction of the Λ [1] and the ϕ [11] that the photon behaves just like a meson. The cross sections are smaller than the corresponding pion cross sections by the factor expected from vector dominance and when the quark fusion models, which successfully describe the hadron data, are applied to the photoproduction data, the shape of the effective photon structure function is indistinguishable from that of the pion[11].

Consequently we can discuss our present data in the light of the quark and diquark fusion models which have been proposed for baryon production in hadron-hadron collisions[12-15]. No specific predictions exist so far for the hyperon and antihyperon data considered here, but it is possible to use the general ideas to give a qualitative explanation of the general features of our data.

From Figs. 6 and 7 we see that the average value of Feynman x for the produced hyperon or antihyperon is $\langle x_F \rangle \simeq 0.15$–$0.20$. With the photon energies and hyperon masses involved, this means that the average fraction of the beam momentum carried by a beam quark or diquark in the fusion process is $\langle x_B \rangle \simeq 0.29$ and the average fraction of the target momentum carried by a target quark or diquark is $\langle x_T \rangle \simeq 0.09$ *). This latter value is sufficiently small to exclude any contribution from valence diquarks in the proton whose distribution is peaked towards large x_T [16,17]. Further, since we are considering beam fragmentation into baryons rather than target fragmentation, it is reasonable to restrict our discussion to the fusion of diquarks from the beam with quarks from the target.

Considering the photon as a superposition of vector mesons, then the diquarks in the beam will be formed primarily from the combination of a valence quark and a sea quark. Restricting ourselves to the ρ, ω, and ϕ,

*) To obtain the values for x_B and x_T we used the relations $x_F = x_B - x_T$, $x_B x_T = M^2/s$, where M is the mass of the hyperon considered.

taking them in the standard ratio of 9:1:2 and assuming that the probability of finding an s-quark in the sea is half that of finding a u- or d-quark in the sea, then it is straightforward to show that

$$\sigma(\gamma p \to \Sigma^0) \propto \frac{27}{20} V_N + \frac{7}{5} S_N$$

$$\sigma(\gamma p \to \overline{\Sigma^0}) \propto \frac{7}{5} S_N$$

$$\sigma(\gamma p \to \Sigma^+) \propto \frac{9}{5} V_N + \frac{7}{5} S_N$$

$$\sigma(\gamma p \to \overline{\Sigma^+}) \propto \frac{7}{5} S_N$$

$$\sigma(\gamma p \to \Sigma^-) \propto \frac{9}{10} V_N + \frac{7}{5} S_N$$

$$\sigma(\gamma p \to \overline{\Sigma^-}) \propto \frac{7}{5} S_N$$

$$\sigma(\gamma p \to \Xi^-) \propto \frac{1}{5} V_N + \frac{13}{20} S_N$$

$$\sigma(\gamma p \to \overline{\Xi^-}) \propto \frac{13}{20} S_N$$

where V_N and S_N are, respectively, the values of the valence and sea quark distributions of the nucleon at the mean value of x_T.

To obtain an estimate of the relative magnitude of the various cross sections, we have used the distributions from Moore[18] which provide a good description of the low-Q^2 data in deep inelastic scattering. However, our results are not particularly sensitive to this choice. The model estimates and the corresponding experimental results are given in Table 3, and show surprising agreement.

6. SEARCH FOR HIGH MASS HYPERON STATES (MASS > 2.0 GeV)

We have looked for high mass hyperon resonances in decay channels containing a $\Lambda(\bar{\Lambda})$ and charged or neutral pions, or $K^- p \pi^\pm$ [reactions (9)-(12) in Table 1]. Weak signals are observed in $\Lambda(3\pi)^\pm$ and $K^- p \pi^\pm$ at a mass around 2.26 GeV, as shown in Fig. 11. The curves in Figs. 11c and f correspond to fits with a Breit-Wigner resonance term and a polynomial background where the width of the signal is fixed to Γ = 0.05 GeV. The fits give consistently a mass value of 2.26 ± 0.06 GeV. The statistical significance is 3σ in both cases.

The weak signals in $K^-p\pi^+$ and $\Lambda\pi^+\pi^+\pi^-$ (Figs. 11a and d) are near to the mass of the charmed baryon Λ_c^+ [2.28 GeV [19)]]. However, similar signals are also visible in the channels $K^-p\pi^-$ and $\Lambda\pi^+\pi^-\pi^-$ (Fig.s 11b and e), indicating that a hyperon state with isospin I = 1, already discussed in other experiments[19)], could be present in our data.

Assuming that the fitted signal in Fig. 11c measures the hyperon candidate only, we calculate an upper limit for the production of Λ_c^+ in $K^-p\pi^+$ as 315 nb with 90% confidence level. It is in good agreement with our earlier estimate[20)], based on a subsample of events containing an additional K^+ (probably from a $\bar{D}$ decay) in the final state.

7. INCLUSIVE PRODUCTION OF $\Lambda\bar{\Lambda}$, $\Lambda\bar{p}$ AND $\bar{\Lambda}p$ PAIRS

In small subsamples of our experimental data we have measured hyperons and antihyperons in inclusive production processes of baryon-antibaryon pairs, i.e. in the reactions (6), (7), and (8) (see Table 1).

The selection and the kinematical range for both Λ and $\bar{\Lambda}$ are the same as for the single particle inclusive production discussed before (i.e. $x_F > -0.3$, see Section 3). Protons and antiprotons are restricted to have momenta in the range $18 < p < 34$ GeV due to their identification by the Cerenkov counter and are thus limited to $x_F > 0.2$.

The number of events observed in the reaction channels (6)-(8) are collected in Table 4, together with estimates of background concerning the protons (antiprotons) due to the inefficiency of the Cerenkov counter, and the corresponding cross sections (orders of magnitude only). The cross section for inclusive $\Lambda\bar{\Lambda}$ production is about 40 nb, and we observe that the cross sections for $\Lambda\bar{p}$ and $\bar{\Lambda}p$ production are about the same and account for $\sim$ 10 nb.

In Fig. 12a we show the added mass distributions of $\Lambda\pi^+$ and $\Lambda\pi^-$ for $\Lambda\bar{\Lambda}$ events. The $\bar{\Sigma}_{1385}$ is clearly visible, demonstrating that production of excited hyperons is also important here. A corresponding $\Lambda\bar{\Sigma}_{1385}$ is not seen in the $\bar{\Lambda}\pi^\pm$ distribution (Fig. 12b). A similar asymmetry in particle-antiparticle production is observed in the reaction channel $\gamma p \to p\bar{p} + X$ where Δ_{1232} and $\bar{\Delta}_{1232}$ production was studied in the forward direction[23)].

Assuming that the hyperons and antihyperons in these events are mainly produced independently of each other, they should show more or less the behaviour seen in the single inclusive studies of Λ and $\bar{\Lambda}$ [1]; an excess of Σ_{1385} production over $\bar{\Sigma}_{1385}$ would thus be expected (see Section 5.2 and Table 3). Furthermore, their x_F distributions should then be similar to the single produced $\Lambda(\bar{\Lambda})$ and concentrate in the central region. The raw data are shown in Figs. 13a and b in comparison with the single $\Lambda(\bar{\Lambda})$ distributions (dotted lines). We note that the x_F distributions of the $\Lambda(\bar{\Lambda})$ from $\Lambda\bar{p}(\bar{\Lambda}p)$ also exhibit this behaviour (dashed lines in Figs. 13a and b); however, no clear $\Sigma_{1385}(\bar{\Sigma}_{1385})$ signals are observed in these channels. Another indication for uncorrelated production of the Λ and $\bar{\Lambda}$ in our $\Lambda\bar{\Lambda}$ events is the absence of any evident structure in the invariant $\Lambda\bar{\Lambda}$ mass distribution.

8. SUMMARY

From our study of inclusive photoproduction of hyperons and antihyperons in the photon energy range of 20 to 70 GeV we note the following facts:

i) $\sigma(\Sigma_{1385}) > \sigma(\bar{\Sigma}_{1385})$ by a factor of 1.4 ± 0.1.

ii) $\sigma(\Xi^-)/\sigma(\Sigma^-_{1385}) = 0.32 \pm 0.06$.

iii) The production of $\overline{\Sigma^0}$, $\overline{\Sigma^+_{1385}}$, and $\overline{\Sigma^=_{1385}}$ is in the order of 20 to 40% of the particle production.

iv) $\overline{\Sigma^+_{1385}}$ and $\overline{\Sigma^=_{1385}}$ are produced about equally.

v) No hyperon or antihyperon production is observed for $x_F > 0.7$.

These results are in surprisingly good agreement with predictions from a quark fusion model [13], which has been proposed for baryon production in hadron-hadron collisions.

The inclusive production of $\Sigma^{\pm}_{1385}$ is also observed in events containing a $\Lambda\bar{\Lambda}$ pair. An uncorrelated production of Λ and $\bar{\Lambda}$ in these events seems to be present in our data.

We wish to express our thanks to the Omega group at CERN for their help in running the spectrometer and providing online and offline software. We have also benefitted from the work of technical support staff at our home institutions. We thank the SERC (UK), BMFT (W. Germany), and the IN2P3 (France) for their financial support.

REFERENCES

1) D. Aston et al., CERN-EP/81-109, to be published in Nucl. Phys. B.

2) F. Barreiro et al., Phys. Rev. D 17 (1978) 669.

3) E. Balea et al., Nucl. Phys. B150 (1979) 345.

4) M. Barradin-Otwinowska et al., Nucl. Phys. B90 (1975) 397.

5) H. Graessler et al., Nucl. Phys. B118 (1977) 189.

6) H. Kichimi et al., Phys. Lett. 72B (1978) 411.

7) M. Bourquin et al., Z. Phys. C 5 (1980) 275.

8) J. Canter et al., Phys. Rev. D 20 (1979) 1029.

9) D. Aston et al., Nucl. Phys. B166 (1980) 113.

10) P. Roudeau, Thèse, Orsay N de ordre 23/5, 1980.

11) D. Aston et al., Nucl. Phys. B179 (1981) 215.

12) V.V. Kniazev et al., Serpukhov IHEP (1977) 77-106.

13) A. Donnachie, Z. Phys. C 4 (1980) 161.

14) V.V. Anisovich and V.M. Shekhter, Nucl. Phys. B55 (1973) 455.

15) Y.V. Fisjak and E.P. Kistenev, CERN-EP/80-209.

16) L.F. Abbot, E.L. Berger, R. Blankenbecler and G. Kane, Phys. Lett. 88B (1979) 157.
L.F. Abbot, W.B. Atwood and R.M. Barnett, Phys. Rev. D 22 (1980) 582.

17) A. Donnachie and P.V. Landshoff, Phys. Lett. 95B (1980) 437.

18) R. Moore, J. Phys. G 5 (1979) 1509.

19) C. Bricman et al., Rev. Mod. Phys. 52 Nr. 2 (1980).

20) D. Aston et al., Phys. Lett. 94B (1980) 113.

21) S. Lichtman et al., Nucl. Phys. B105 (1976) 229.

22) D. Bogert et al., Phys. Rev. D 16 (1977) 2089.

23) C. Steinhauer, Thesis, Bonn 1981, in preparation.

Table 1

Reactions of inclusive baryon and antibaryon productions considered in this paper

$\gamma p \to \ldots + X$	$\gamma p \to \ldots + X$	
$\Sigma^0 \to \Lambda\gamma$	$\overline{\Sigma^0} \to \bar{\Lambda}\gamma$	(1)
$\Sigma^+_{1385} \to \Lambda\pi^+$	$\overline{\Sigma^+_{1385}} \to \bar{\Lambda}\pi^-$	(2)
$\Sigma^-_{1385} \to \Lambda\pi^-$	$\overline{\Sigma^-_{1385}} \to \bar{\Lambda}\pi^+$	(3)
$\Xi^0 \to \Lambda\pi^0$	$\overline{\Xi^0} \to \bar{\Lambda}\pi^0$	(4)
$\Xi^- \to \Lambda\pi^-$	$\overline{\Xi^-} \to \bar{\Lambda}\pi^+$	(5)
$\gamma p \to \Lambda\bar{\Lambda} + X$	$\gamma p \to \Lambda\Lambda + X$	(6)
$\gamma p \to \Lambda\bar{p} + X$	$\gamma p \to \Lambda p + X$	(7)
$\gamma p \to \bar{\Lambda} p + X$		(8)
$\gamma p \to p K^- \pi^+ + X$		(9)
$\gamma p \to p K^- \pi^- + X$		(10)
$\gamma p \to \Lambda(3\pi)^+ + X$		(11)
$\gamma p \to \Lambda(3\pi)^- + X$		(12)

Table 2

Cross section estimates for various reactions. The cross sections are an average over the photon energy range 20-70 GeV weighted by the bremsstrahlung spectrum $1/E_\gamma$.

	Number of events	Acceptance*)	x_F range	Cross section**) (nb)
Σ^+_{1385}	$891\ ^{+\ 38}_{-\ 130}$	0.066	> -0.3	135 ± 45
Σ^-_{1385}	653 ± 37	0.066	> -0.3	100 ± 30
$\overline{\Sigma^+_{1385}}$	262 ± 23	0.066	> -0.3	37 ± 15
$\overline{\Sigma^-_{1385}}$	196 ± 24	0.066	> -0.3	28 ± 10
Ξ^-	160 ± 28 (a)***) 50 ± 18 (b)	0.075	> -0.3	28 ± 9
$\overline{\Xi^-}$	48 ± 15	0.053	> -0.3	9 ± 4

*) Includes all corrections for various losses, also branching ratio.

**) Error includes the uncertainty of acceptance.

***) First (a) and second (b) sample of Ξ^- decays (see text).

Table 3

Comparison of model predictions (see text) for specific cross section ratios and the corresponding experimental values

Cross section ratios	Experimental values	Model predictions
$\sigma(\Sigma^+_{1385})/\sigma(\Lambda)$	0.10 ± 0.02	-
$\sigma(\overline{\Sigma^+_{1385}})/\sigma(\bar{\Lambda})$	0.12 ± 0.02	-
$\sigma(\Sigma^+_{1385})/\sigma(\Sigma^-_{1385})$	1.4 ± 0.1	1.56
$\sigma(\overline{\Sigma^+_{1385}})/\sigma(\overline{\Sigma^-_{1385}})$	1.3 ± 0.2	1.00
$\sigma(\overline{\Sigma^0})/\sigma(\Sigma^0)$	0.36 ± 0.06	0.34
$\sigma(\overline{\Sigma^+_{1385}})/\sigma(\Sigma^+_{1385})$	0.27 ± 0.04	0.27
$\sigma(\overline{\Sigma^-_{1385}})/\sigma(\Sigma^-_{1385})$	0.28 ± 0.04	0.42
$\sigma(\overline{\Xi^-})/\sigma(\Xi^-)$	0.32 ± 0.13	0.6
$\sigma(\Xi^-)/\sigma(\Sigma^-_{1385})$	0.28 ± 0.06	0.33

Table 4

Number of events, estimates of background from the Cerenkov counter, and cross sections of reactions (6), (7), and (8). The cross sections are not corrected for backgrounds, and are an average over the photon energy range 20-70 GeV weighted by the Bremsstrahlung spectrum $1/E_\gamma$.

	Number of events	C background	Cross section (nb)
$\Lambda\bar{\Lambda}$	92	-	35
$\Lambda\bar{p}$	111	$\sim$ 13	9
$\bar{\Lambda}p$	121	$\sim$ 5	11
$\Lambda\Lambda$	14	-	7
Λp	110	$\sim$ 16	10

Figure captions

Fig. 1 : Layout of the experiment.

Fig. 2 : a) cos θ distribution of the proton from the Λ decay (small curves show acceptance). Here, θ is the angle of the proton in the Λ rest frame relative to the Λ direction. (Λ with cos θ < -0.96 were rejected because of the high electromagnetic background.

b) cos θ distribution of the π^+ from the $\bar{\Lambda}$ decay (small curves show acceptance). θ is defined above. ($\bar{\Lambda}$ with cos θ > +0.96 were rejected because of the high electromagnetic background.)

Fig. 3 : a) Mass spectrum of Λγ combinations. The curve shows a fit with a Breit-Wigner function plus a background term (see text).

b) Mass spectrum of $\bar{\Lambda}\gamma$ combinations.

Fig. 4 : a) Mass spectrum of $\Lambda\pi^+$.

b) Mass spectrum of $\Lambda\pi^-$.

The curves show fits of Σ^+_{1385}, Σ^-_{1385}, and Ξ^-.

Fig. 5 : a) Mass spectrum of $\bar{\Lambda}\pi^-$.

b) Mass spectrum of $\bar{\Lambda}\pi^+$.

The curves show fits of $\overline{\Sigma^+_{1385}}$, $\overline{\Sigma^-_{1385}}$, and $\overline{\Xi^-}$.

Fig. 6 : $d\sigma(\Sigma^+_{1385})/dx_F$ (a) and $d\sigma(\Sigma^-_{1385})/dx_F$ (b) as a function of x_F. The curve in (a) shows the acceptance for $\Sigma^\pm_{1385}$ and $\overline{\Sigma^\mp_{1385}}$ (see also Section 4).

Fig. 7 : $d\sigma(\overline{\Sigma^\mp_{1385}})/dx_F$ (a) and $d\sigma(\overline{\Sigma^-_{1385}})/dx_F$ (b) as a function of x_F.

Fig. 8 : $d\sigma(\Sigma^+_{1385})/dp_T^2$ and $d\sigma(\Sigma^-_{1385})/dp_T^2$ as a function of p_T^2.

Fig. 9 : $d\sigma(\overline{\Sigma^\mp_{1385}})/dp_T^2$ and $d\sigma(\overline{\Sigma^-_{1385}})/dp_T^2$ as a function of p_T^2.

Fig. 10 : a) Mass spectrum for $\Lambda\pi^0$.

b) Mass spectrum for $\bar{\Lambda}\pi^0$.

Fig. 11 : a) Mass spectrum of $K^-p\pi^+$.

b) Mass spectrum of $K^-p\pi^-$.

c) Sum of (a) and (b).

d) Mass spectrum of $\Lambda\pi^+\pi^+\pi^-$.

e) Mass spectrum of $\Lambda\pi^+\pi^-\pi^-$.

f) Sum of (d) and (e).

Fig. 12 : a) Added mass distributions of $\Lambda\pi^+$ and $\Lambda\pi^-$ from $\Lambda\bar{\Lambda}$ events.

b) Added mass distributions of $\bar{\Lambda}\pi^-$ and $\bar{\Lambda}\pi^+$ from $\Lambda\bar{\Lambda}$ events.

Fig. 13 : x_F distributions of baryons (a) and antibaryons (b), raw data.

—— $\Lambda(\bar{\Lambda})$ from $\Lambda\bar{\Lambda}$

--- $\Lambda(\bar{\Lambda})$ from $\Lambda\bar{p}(\bar{\Lambda}p)$

··· $\Lambda(\bar{\Lambda})$ from the inclusive study[1] (arbitrary normalization).

The acceptance of Λ and $\bar{\Lambda}$ from all three channels exhibit approximately the same behaviour, although they differ in magnitude.

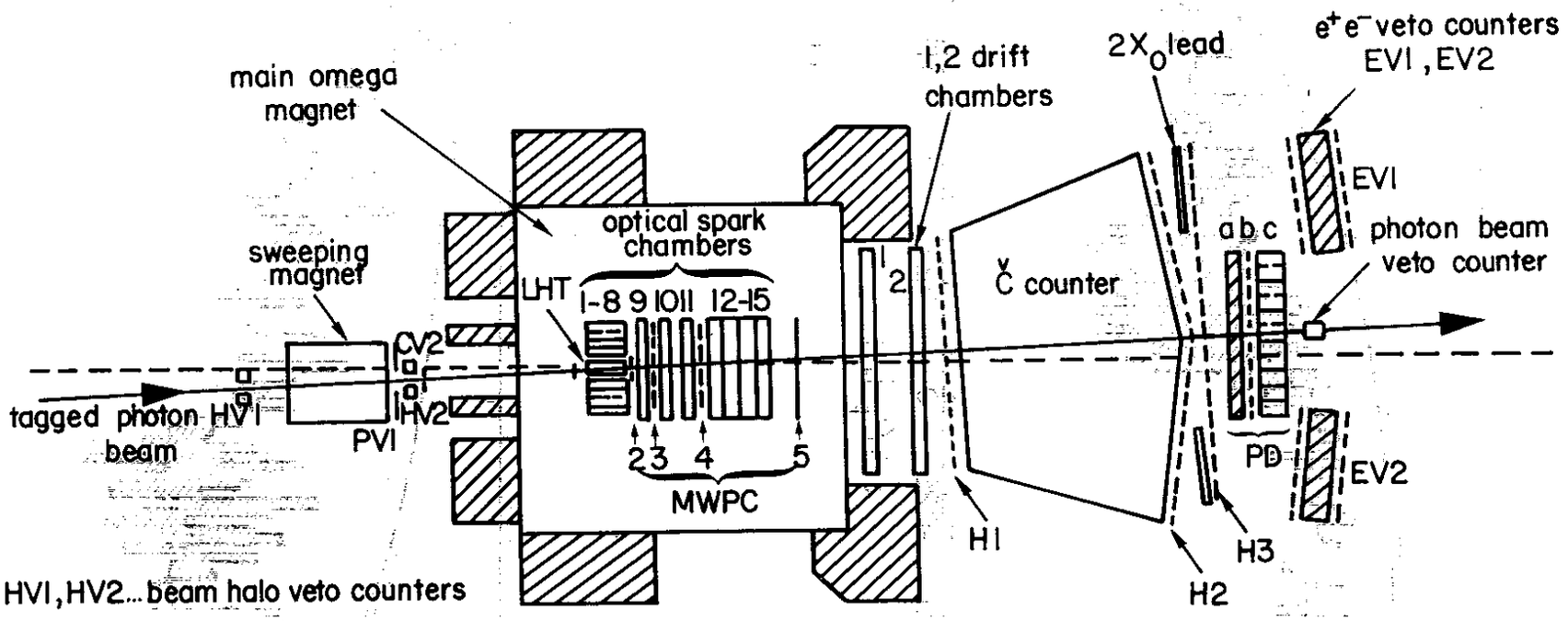
main omega magnet
sweeping magnet
optical spark chambers
LHT
1-8 9 10 11 12-15
1,2 drift chambers
2X0 lead
e+e- veto counters
EV1 , EV2
EV1
a b c
photon beam veto counter
C counter
CV2
HV2
PV1
tagged photon beam
HV1
2 3 4 5
MWPC
H1
H2
H3
PD
EV2
HV1,HV2... beam halo veto counters
PV1,CV2....charged particle veto counter
LHT..... liquid hydrogen target surrounded by scintillator array
H1 , H2, H3.. scintillator hodoscopes
0
5m
PD PHOTON DETECTOR
a) lead glass shower sampler
b) scintillator hodoscopes
c) lead glass array

FIG 1

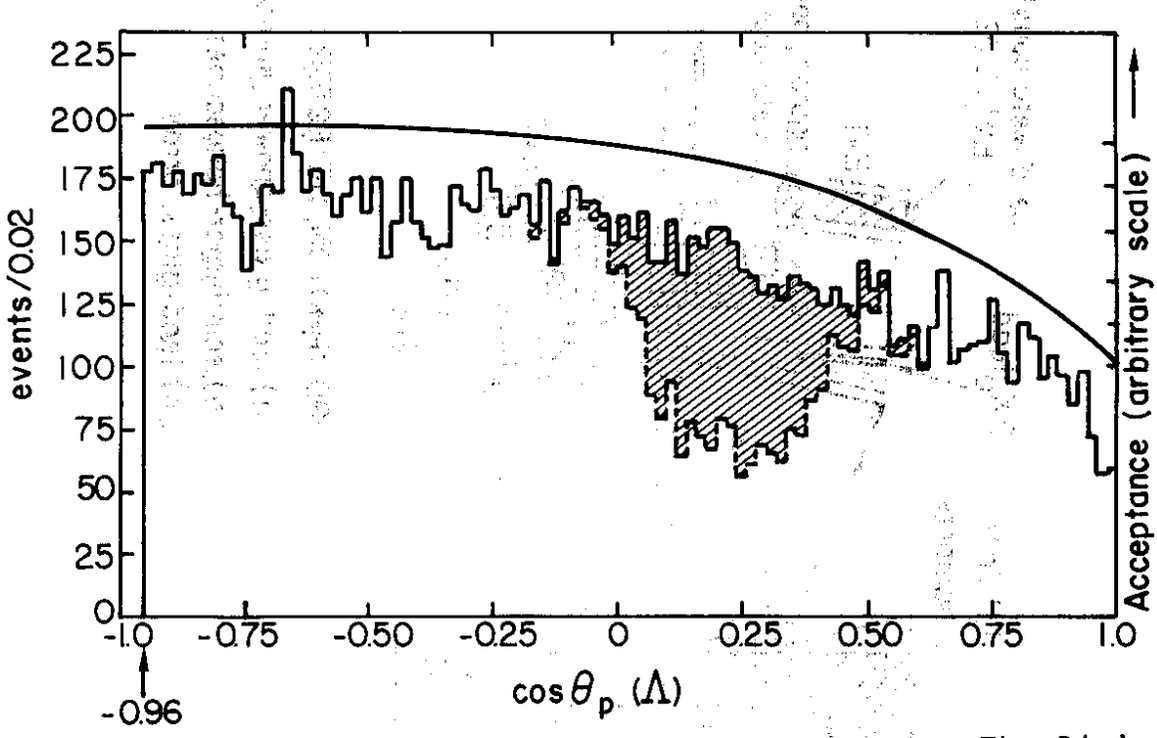
events/0.02
225
200
175
150
125
100
75
50
25
0
-1.0
-0.75
-0.50
-0.25
0
0.25
0.50
0.75
1.0
-0.96
cos θ p (Λ)
Acceptance (arbitrary scale)

Fig. 2(a)

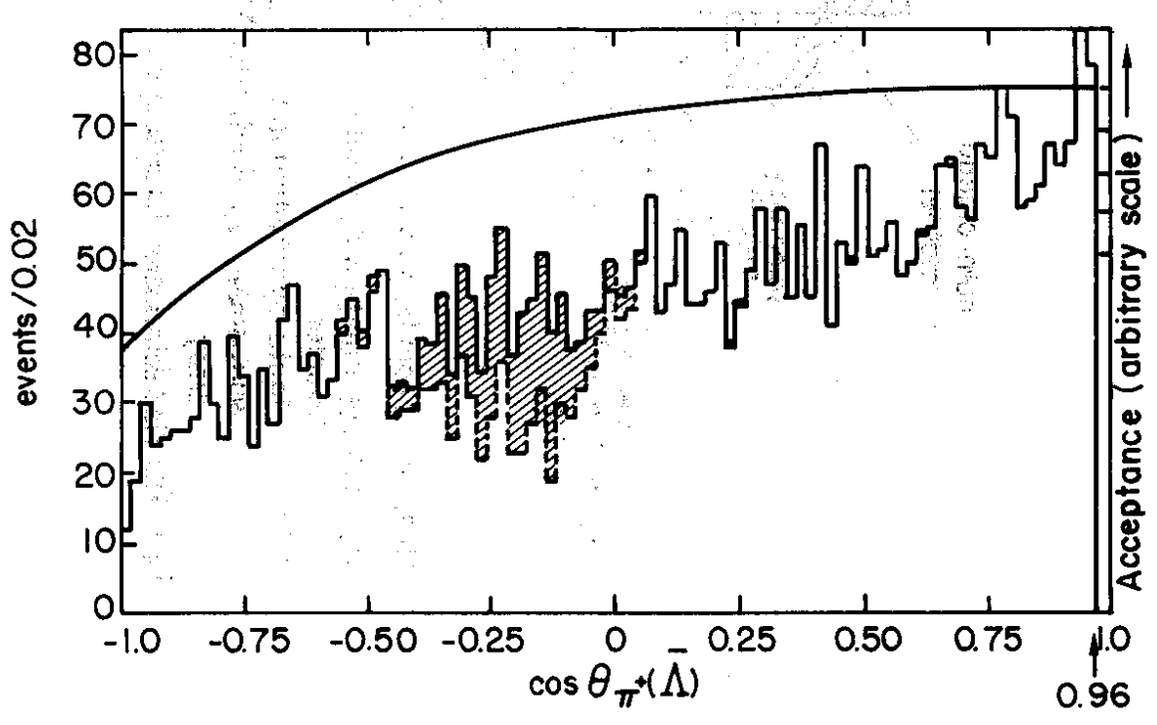
events/0.02
80
70
60
50
40
30
20
10
0
-1.0
-0.75
-0.50
-0.25
0
0.25
0.50
0.75
1.0
0.96
cos θ π+(Λ̄)
Acceptance (arbitrary scale)

Fig. 2(b)

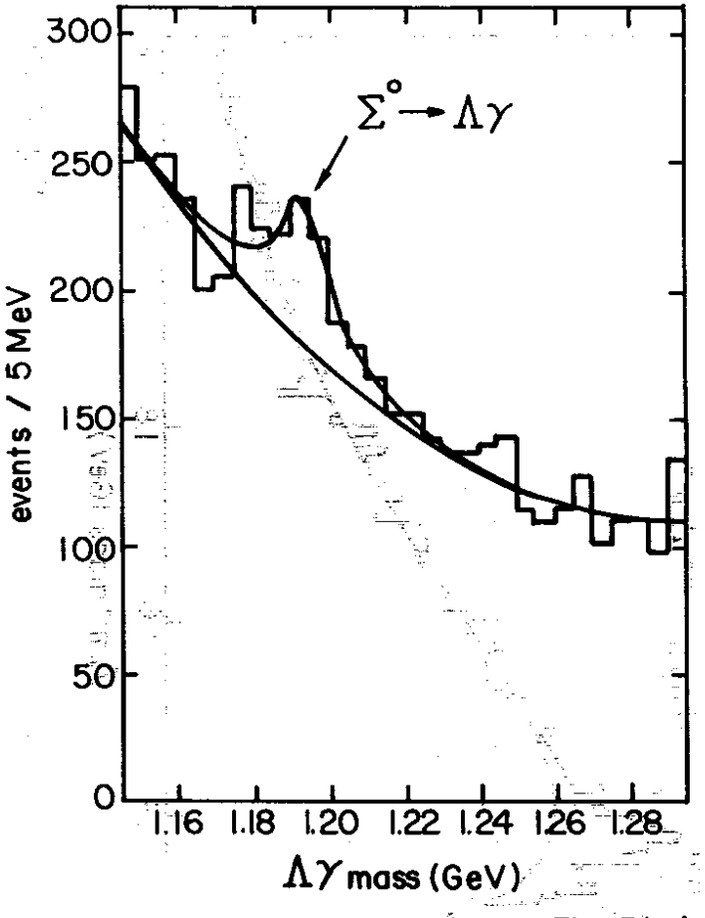
300
250
200
150
100
50
0
events / 5 MeV
$\Sigma^0 \rightarrow \Lambda\gamma$
1.16
1.18
1.20
1.22
1.24
1.26
1.28
$\Lambda\gamma$ mass (GeV)

Fig. 3(a)

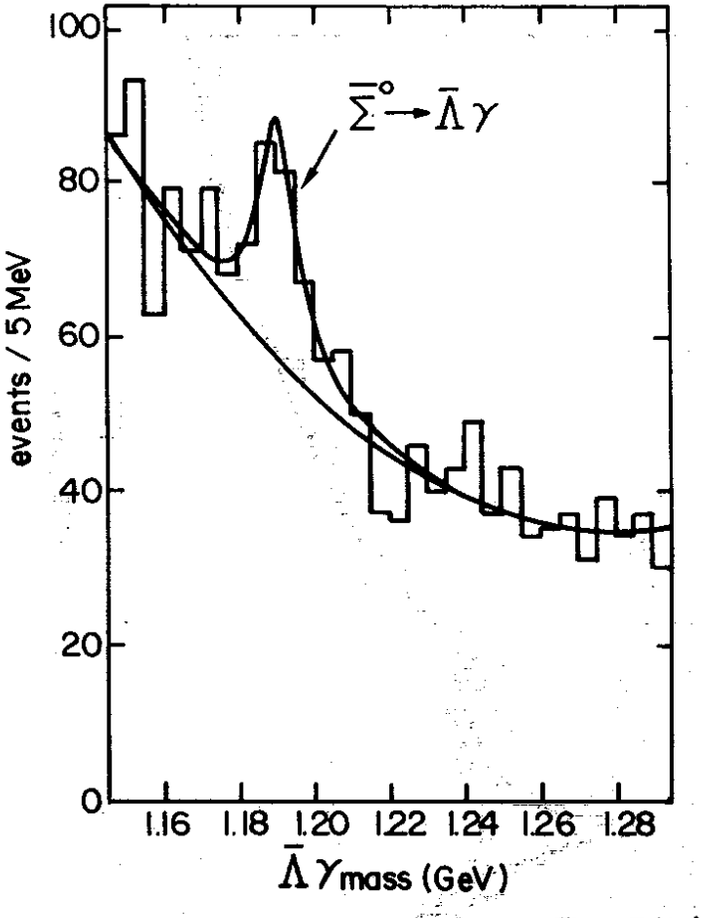
100
80
60
40
20
0
events / 5 MeV
$\bar{\Sigma}^0 \rightarrow \bar{\Lambda}\gamma$
1.16
1.18
1.20
1.22
1.24
1.26
1.28
$\bar{\Lambda}\gamma$ mass (GeV)

Fig. 3(b)

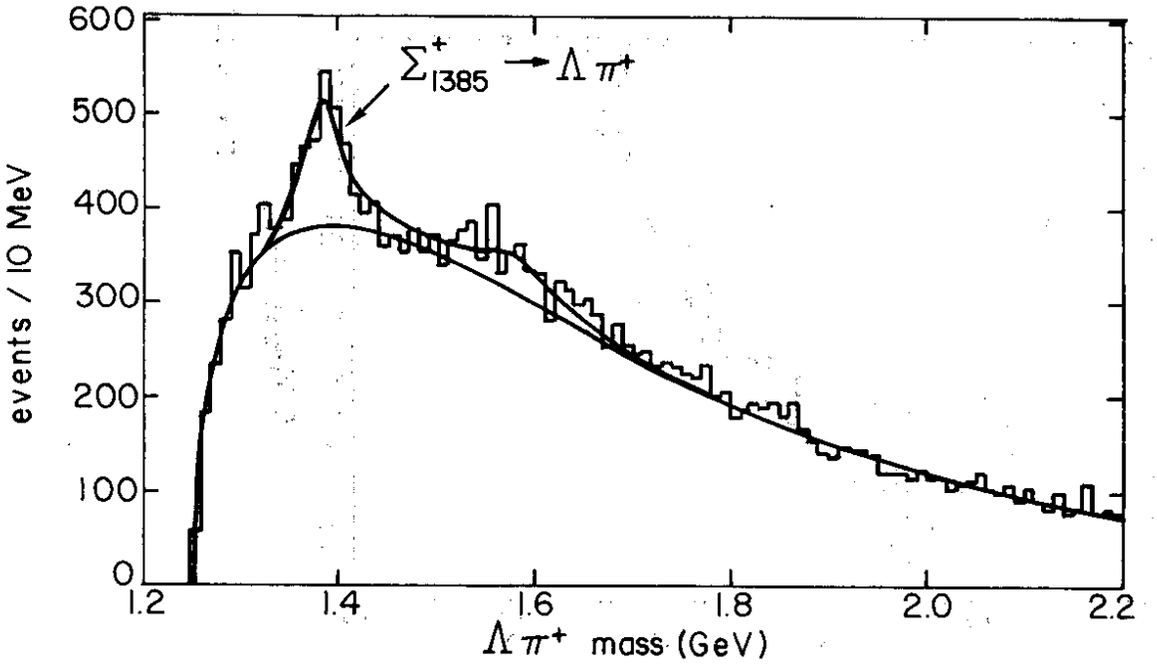
600
500
400
300
200
100
0
events / 10 MeV
$\Sigma^+_{1385} \rightarrow \Lambda\pi^+$
1.2
1.4
1.6
1.8
2.0
2.2
$\Lambda\pi^+$ mass (GeV)

Fig. 4 (a)

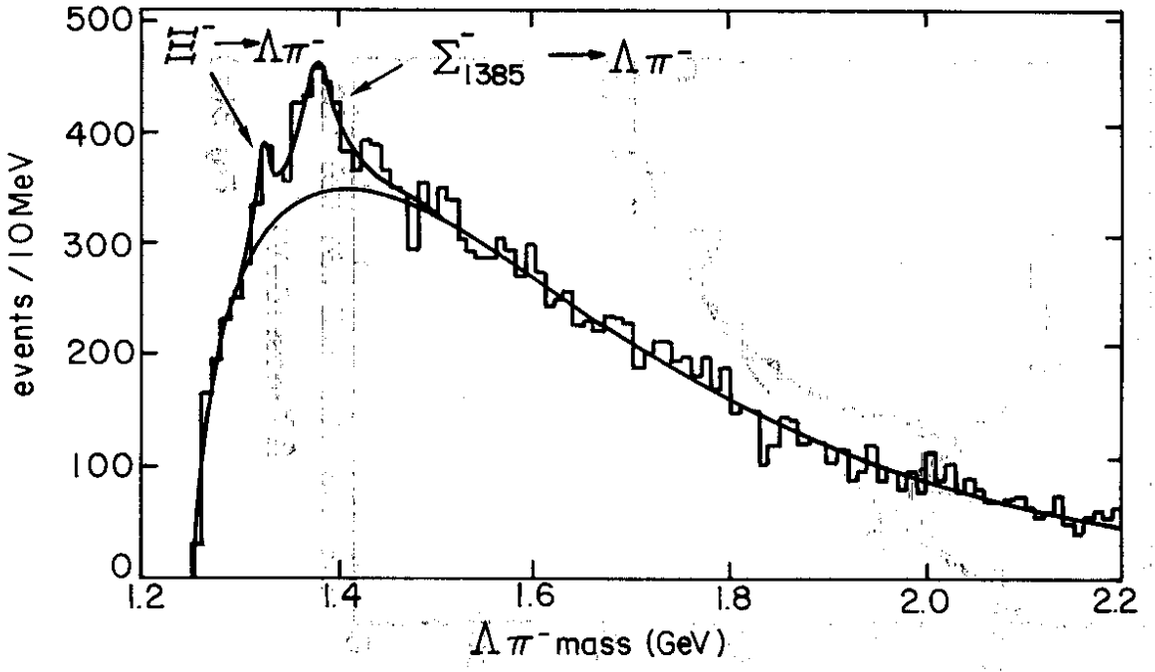
500
400
300
200
100
0
events / 10 MeV
$\Xi^- \rightarrow \Lambda\pi^-$
$\Sigma^-_{1385} \rightarrow \Lambda\pi^-$
1.2
1.4
1.6
1.8
2.0
2.2
$\Lambda\pi^-$ mass (GeV)

Fig. 4 (b)

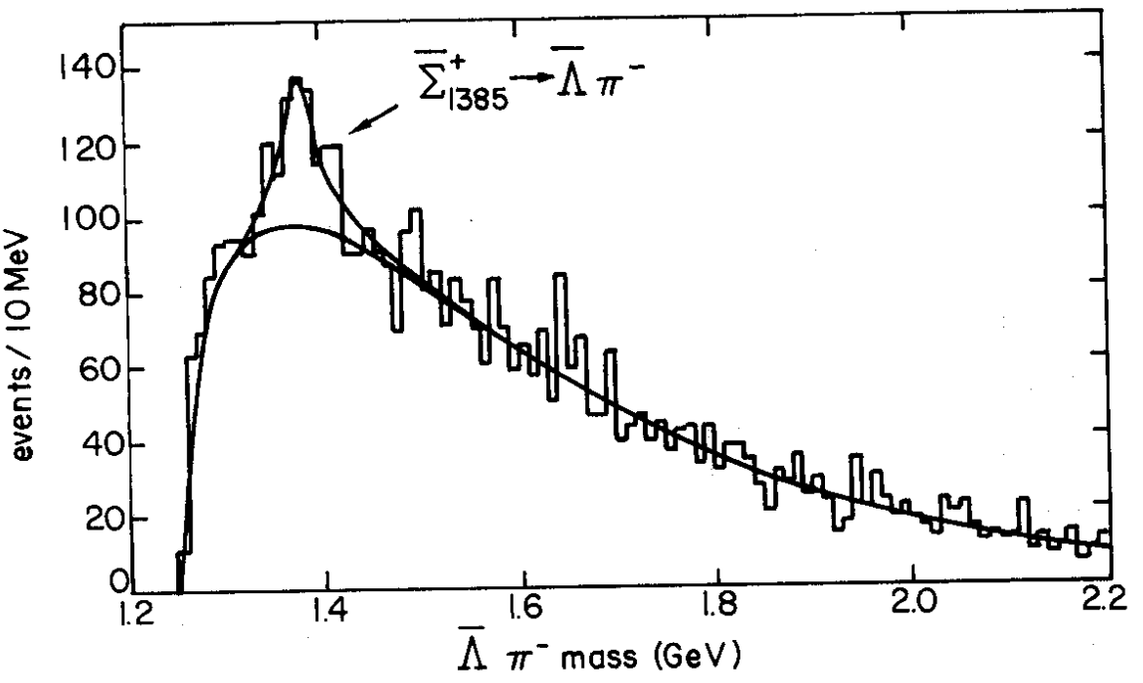
$\overline{\Sigma}^{+}_{1385} \rightarrow \overline{\Lambda}\pi^{-}$
events / 10 MeV
0
20
40
60
80
100
120
140
1.2
1.4
1.6
1.8
2.0
2.2
$\overline{\Lambda}\pi^{-}$ mass (GeV)

Fig. 5 (a)

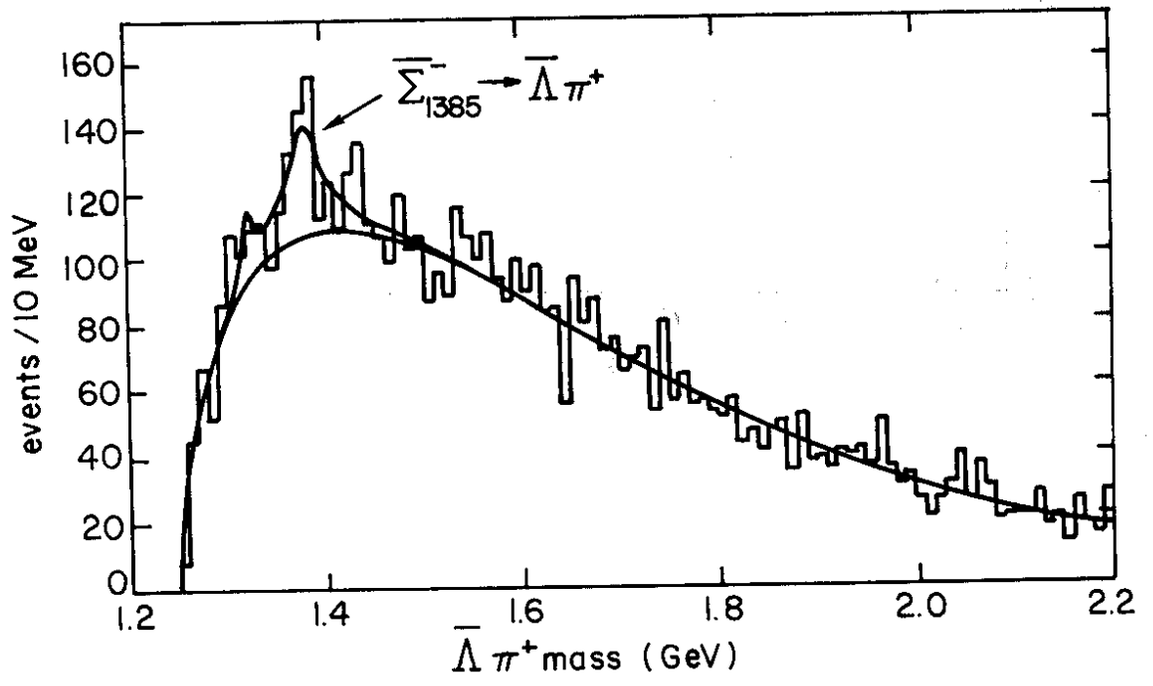
$\overline{\Sigma}^{-}_{1385} \rightarrow \overline{\Lambda}\pi^{+}$
events / 10 MeV
0
20
40
60
80
100
120
140
160
1.2
1.4
1.6
1.8
2.0
2.2
$\overline{\Lambda}\pi^{+}$ mass (GeV)

Fig. 5 (b)

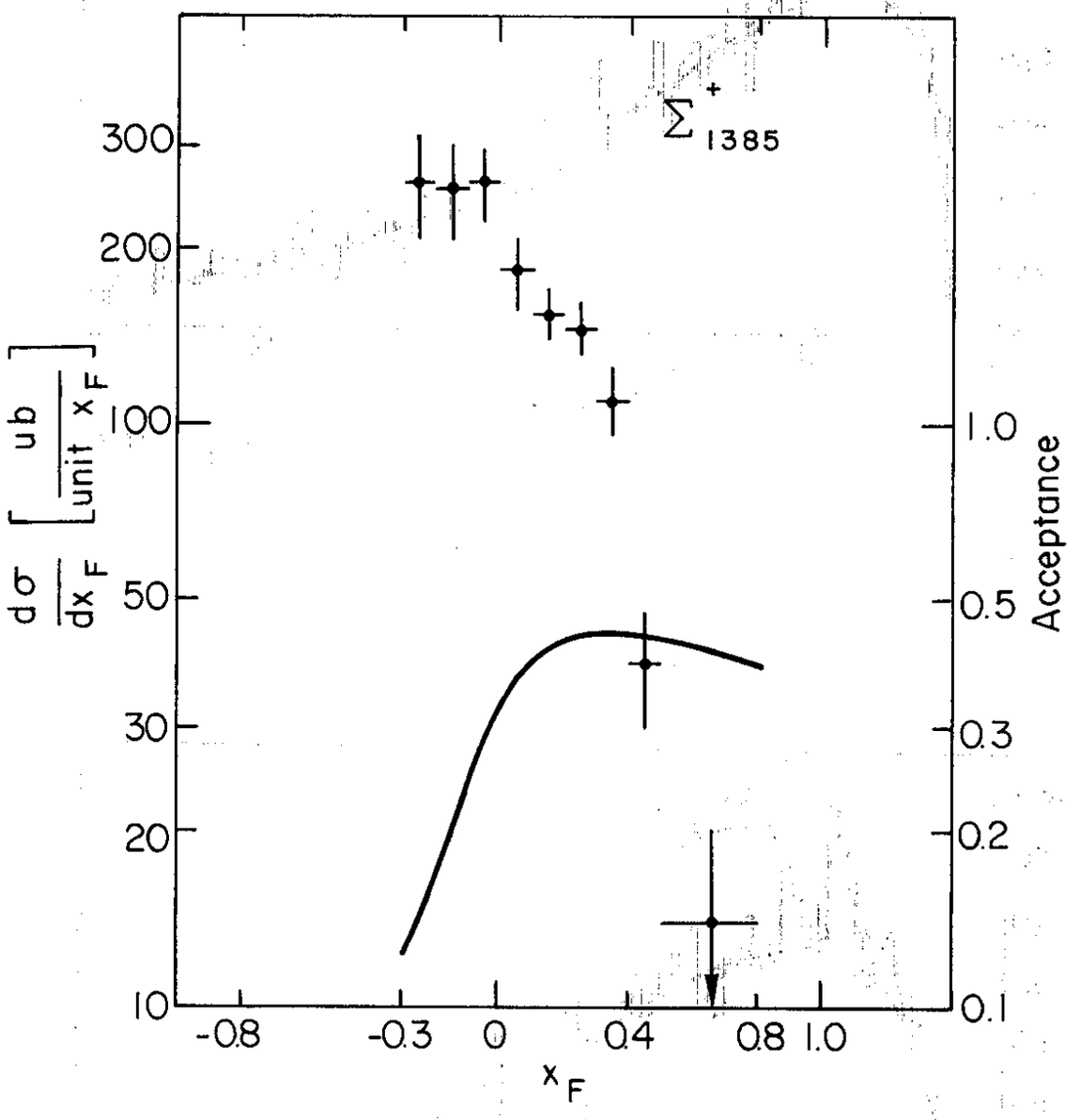
Σ^+_{1385}
300
200
100
50
30
20
10
$\frac{d\sigma}{dx_F}$ $\left[\frac{ub}{unit\ x_F}\right]$
1.0
0.5
0.3
0.2
0.1
Acceptance
-0.8
-0.3
0
0.4
0.8
1.0
x_F

Fig. 6 (a)

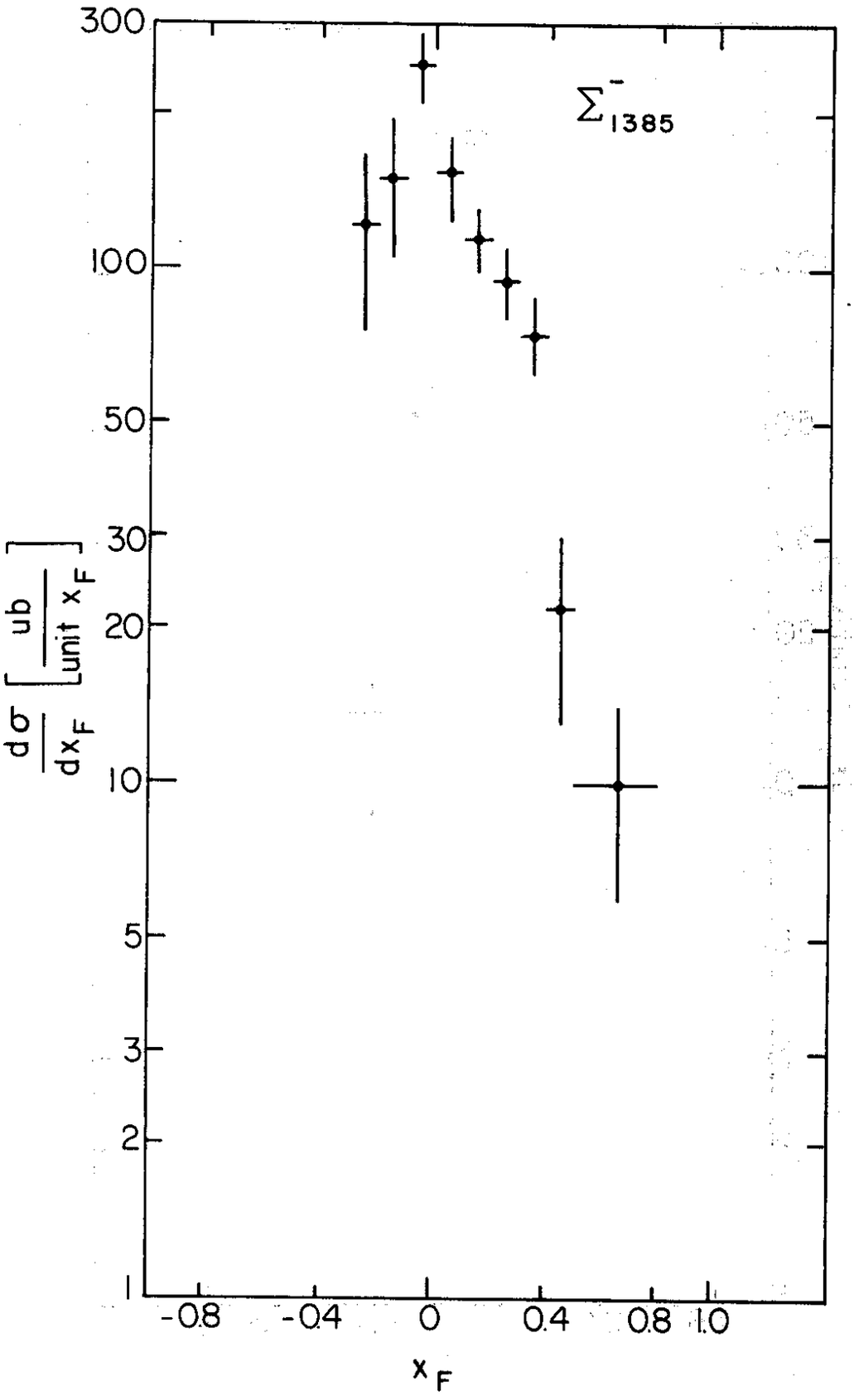
300
100
50
30
20
10
5
3
2
1
Σ^-_{1385}
$\frac{d\sigma}{dx_F}\left[\frac{ub}{unit\ x_F}\right]$
-0.8
-0.4
0
0.4
0.8
1.0
x_F

Fig. 6 (b)

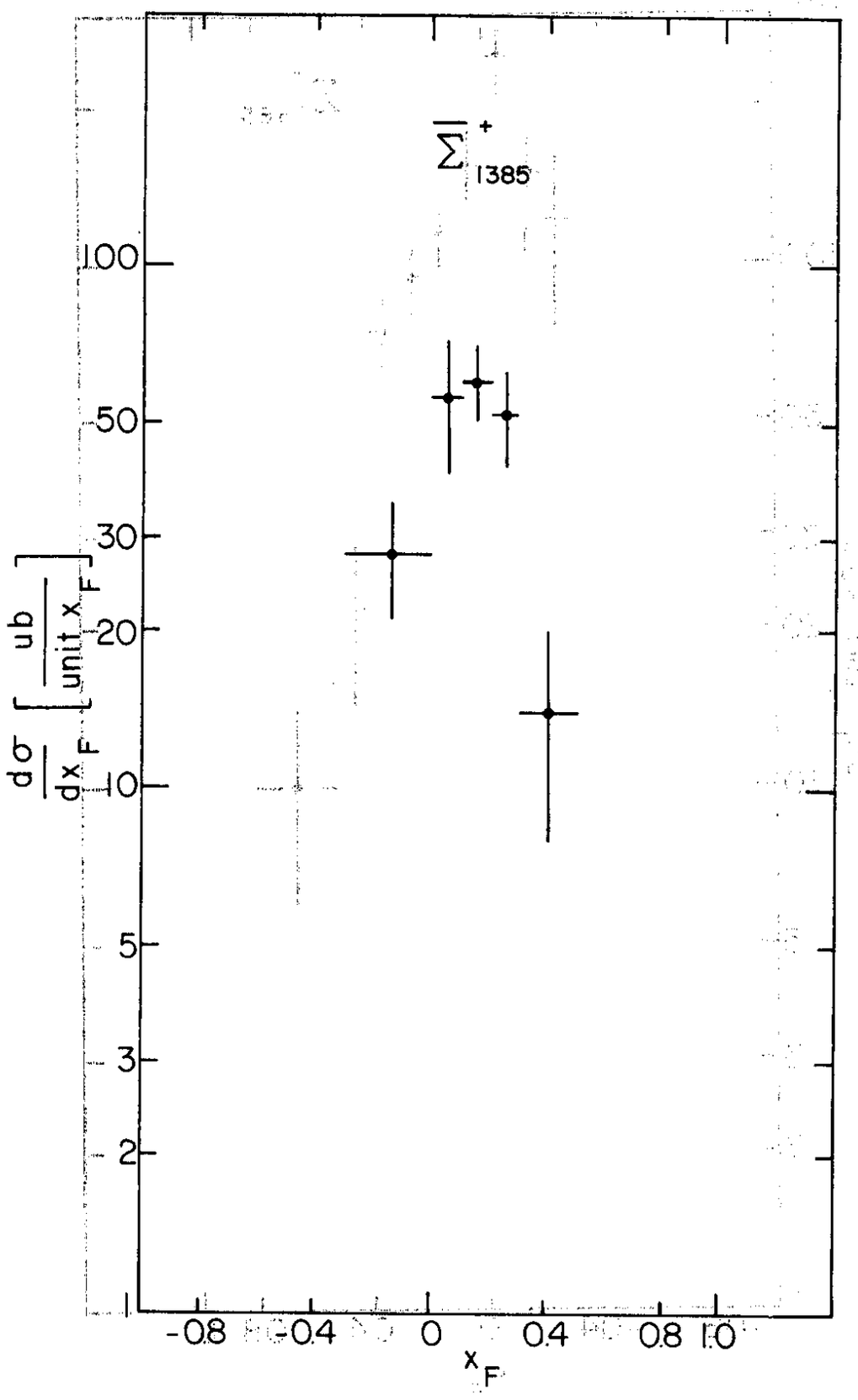
$\bar{\Sigma}^+_{1385}$
100
50
30
20
10
5
3
2
1
$\frac{d\sigma}{dx_F}\left[\frac{ub}{unit\ x_F}\right]$
-0.8
-0.4
0
0.4
0.8
1.0
x_F

Fig. 7 (a)

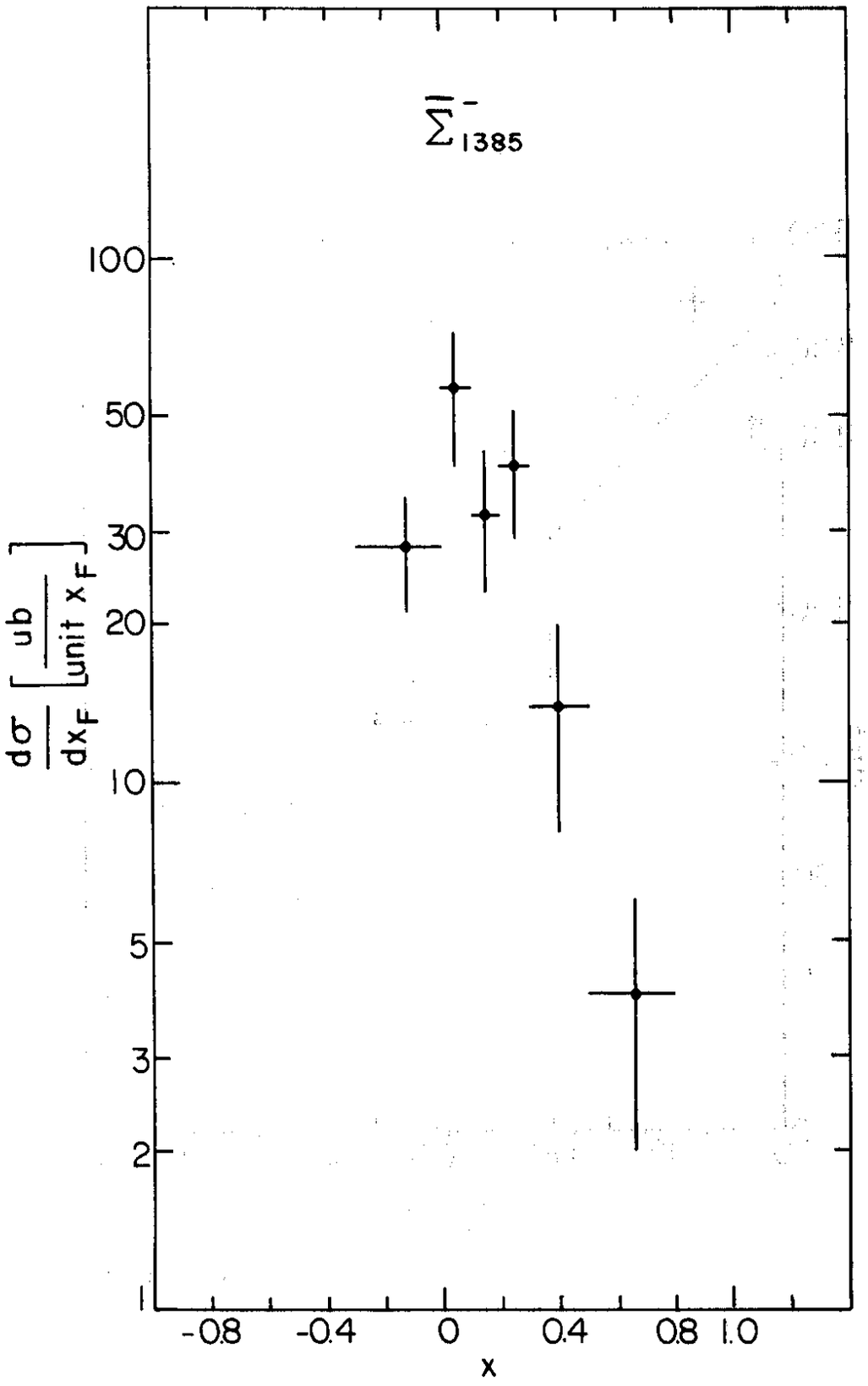
$\bar{\Sigma}^-_{1385}$
100
50
30
20
10
5
3
2
1
$\frac{d\sigma}{dx_F}\left[\frac{ub}{unit\ x_F}\right]$
-0.8
-0.4
0
0.4
0.8
1.0
x

Fig. 7 (b)

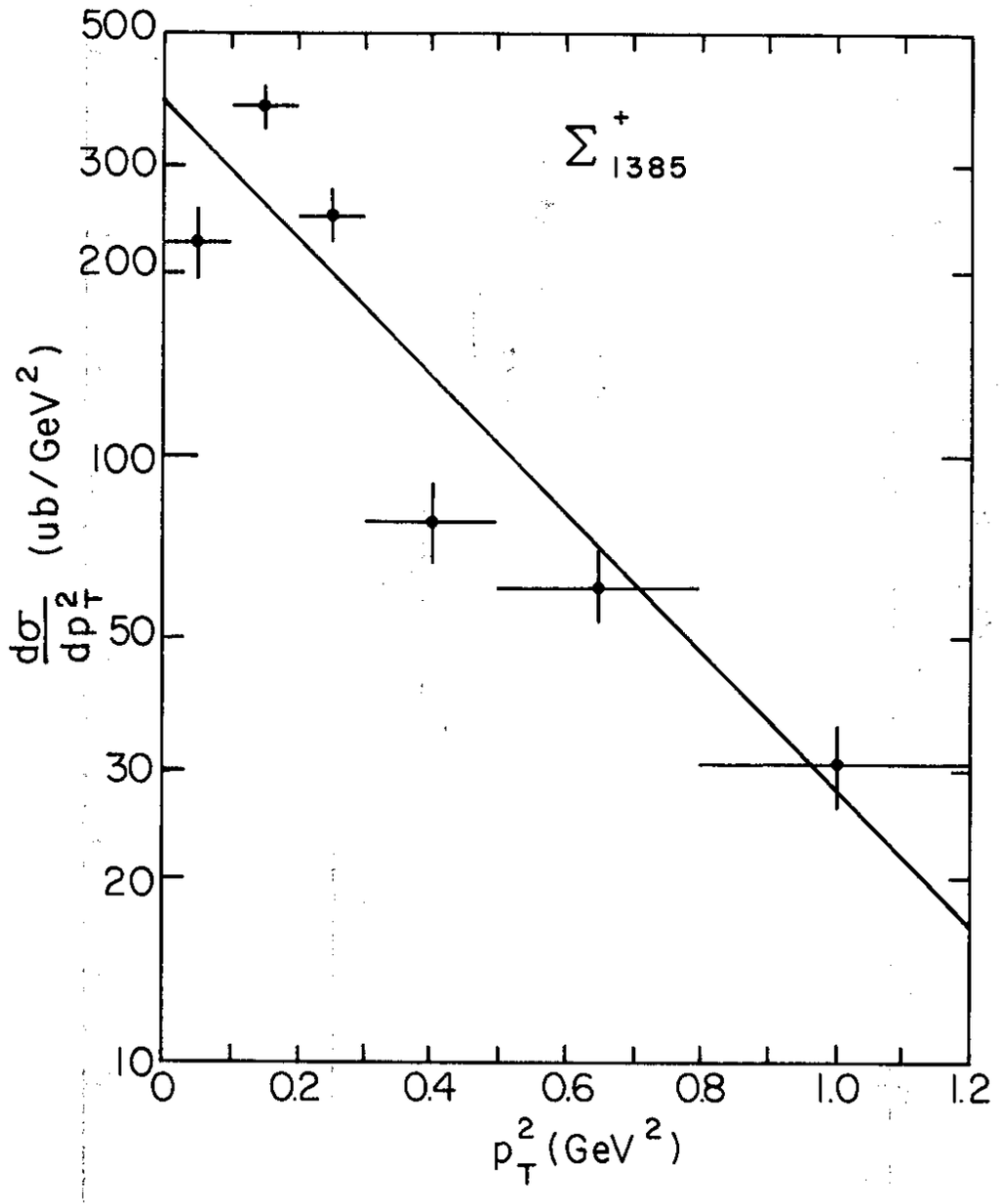
500
300
200
100
50
30
20
10
0
0.2
0.4
0.6
0.8
1.0
1.2
Σ^+_{1385}
$\frac{d\sigma}{dp_T^2}$ (ub/GeV^2)
p_T^2 (GeV^2)

Fig.8 (a)

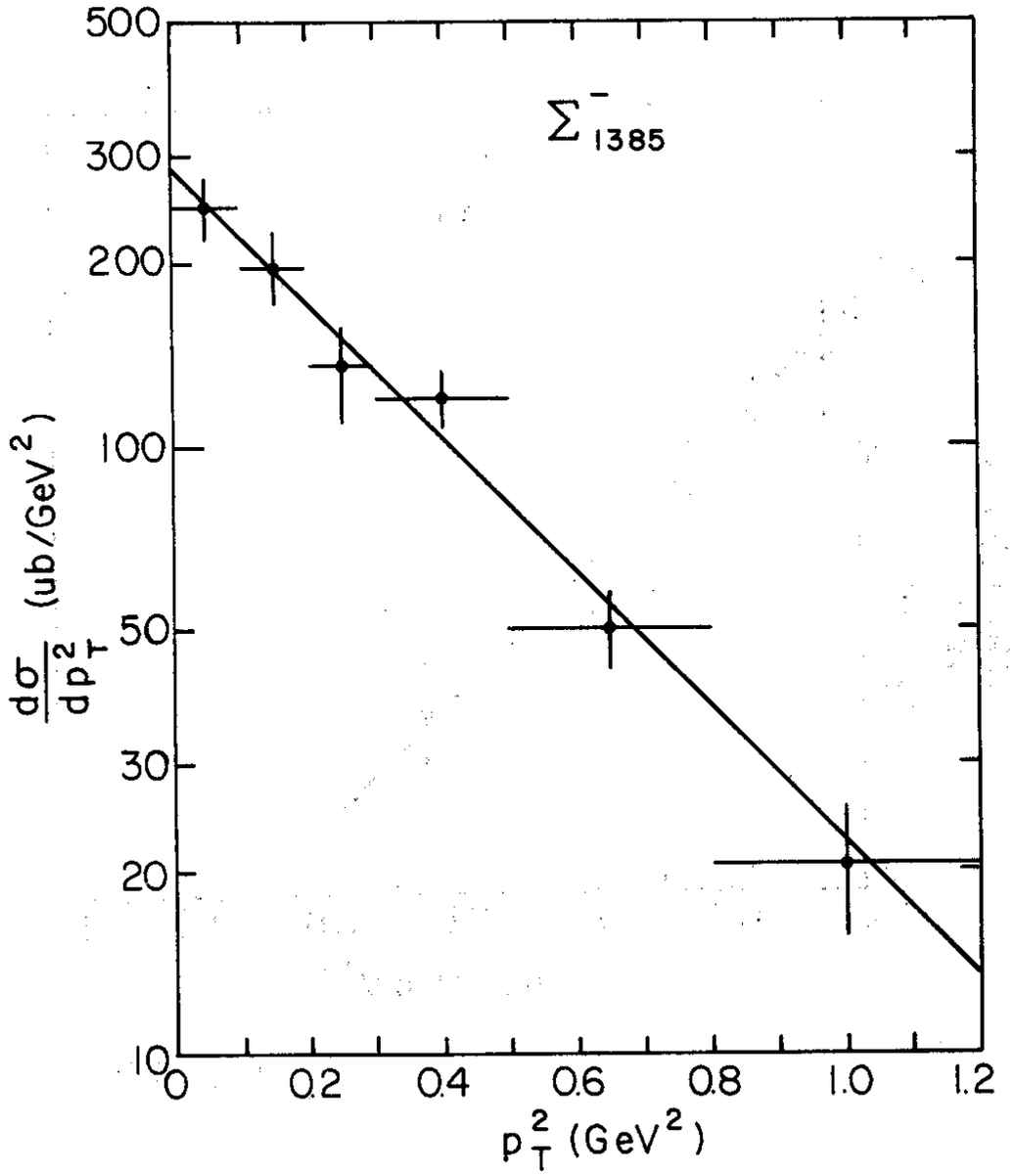
500
300
200
100
50
30
20
10
0
0.2
0.4
0.6
0.8
1.0
1.2
Σ^-_{1385}
$\frac{d\sigma}{dp_T^2}$ (ub/GeV^2)
p_T^2 (GeV^2)

Fig.8 (b)

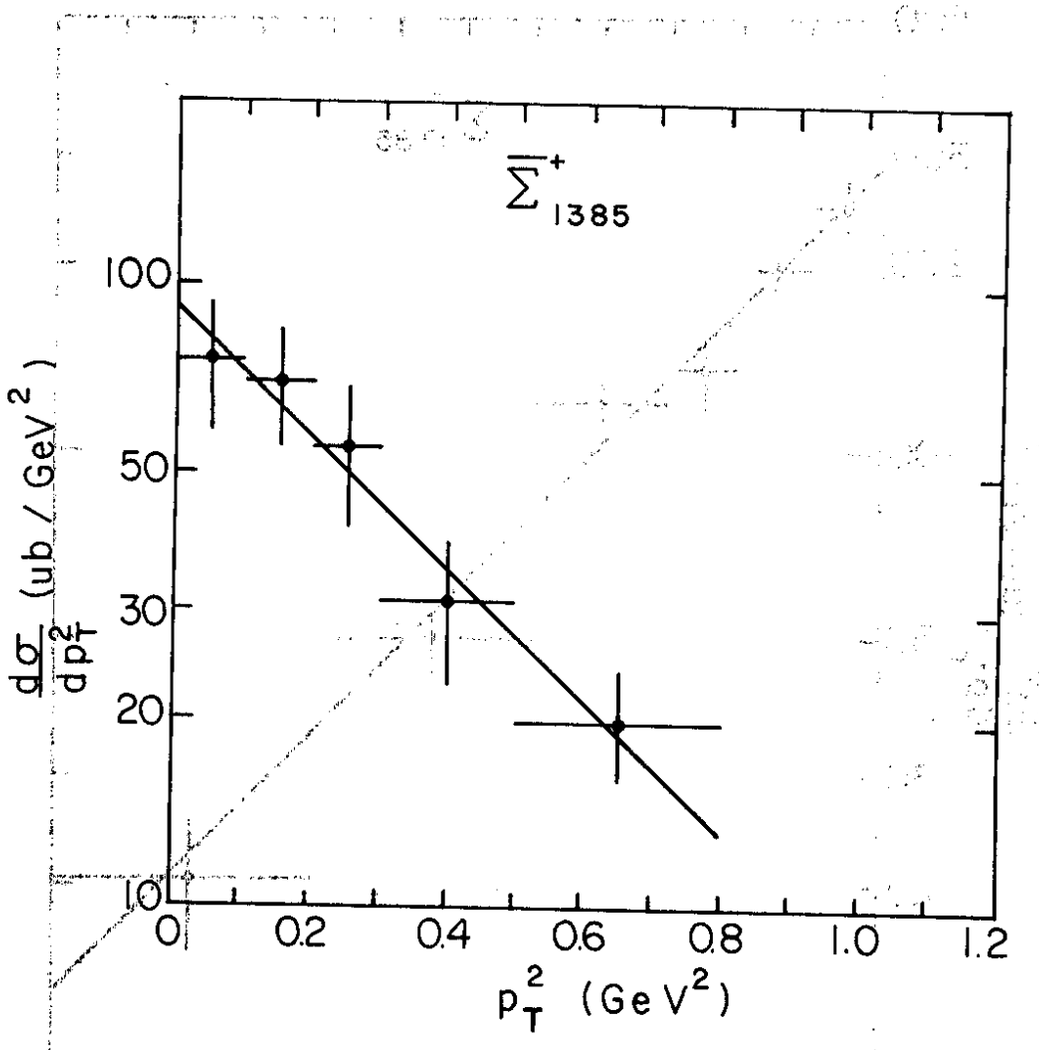
$\bar{\Sigma}^+_{1385}$
100
50
30
20
10
0
0.2
0.4
0.6
0.8
1.0
1.2
$\frac{d\sigma}{dp_T^2}$ (ub / GeV^2)
p_T^2 (GeV^2)

Fig. 9 (a)

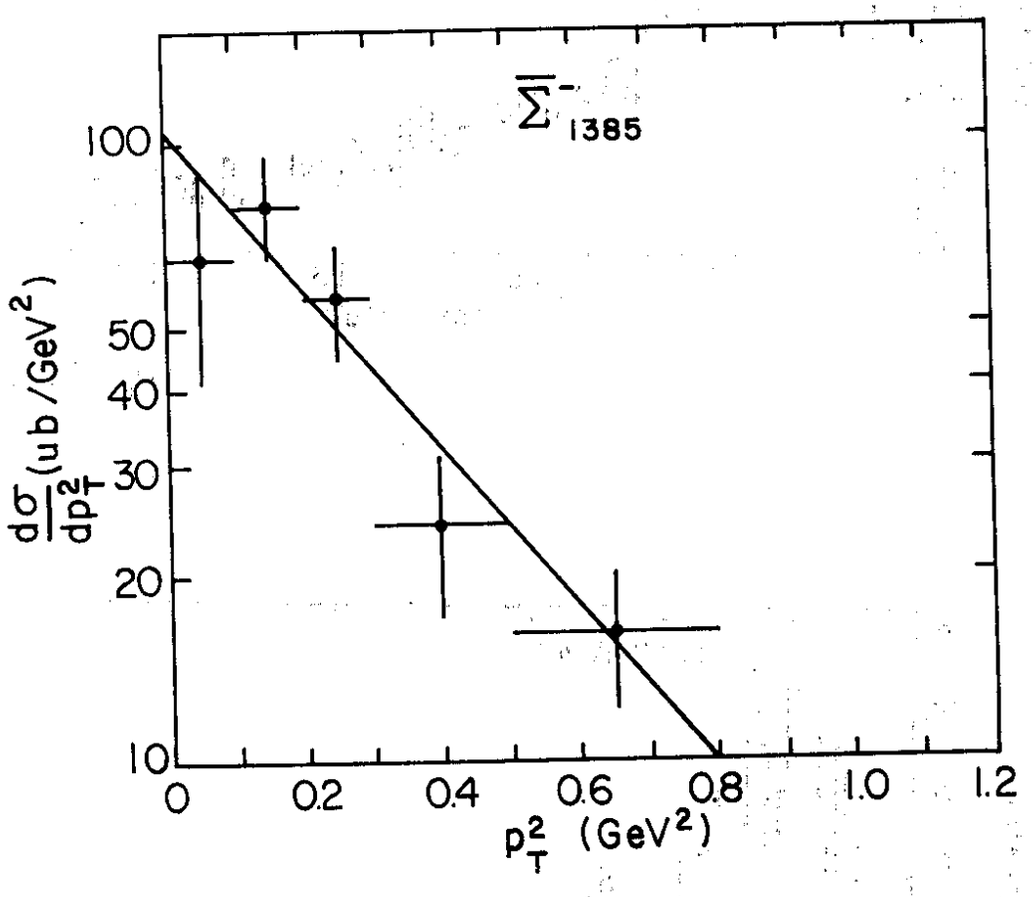
$\overline{\Sigma}^-_{1385}$
100
50
40
30
20
10
$\frac{d\sigma}{dp_T^2}$(ub/GeV^2)
0
0.2
0.4
0.6
0.8
1.0
1.2
p_T^2 (GeV^2)

Fig. 9 (b)

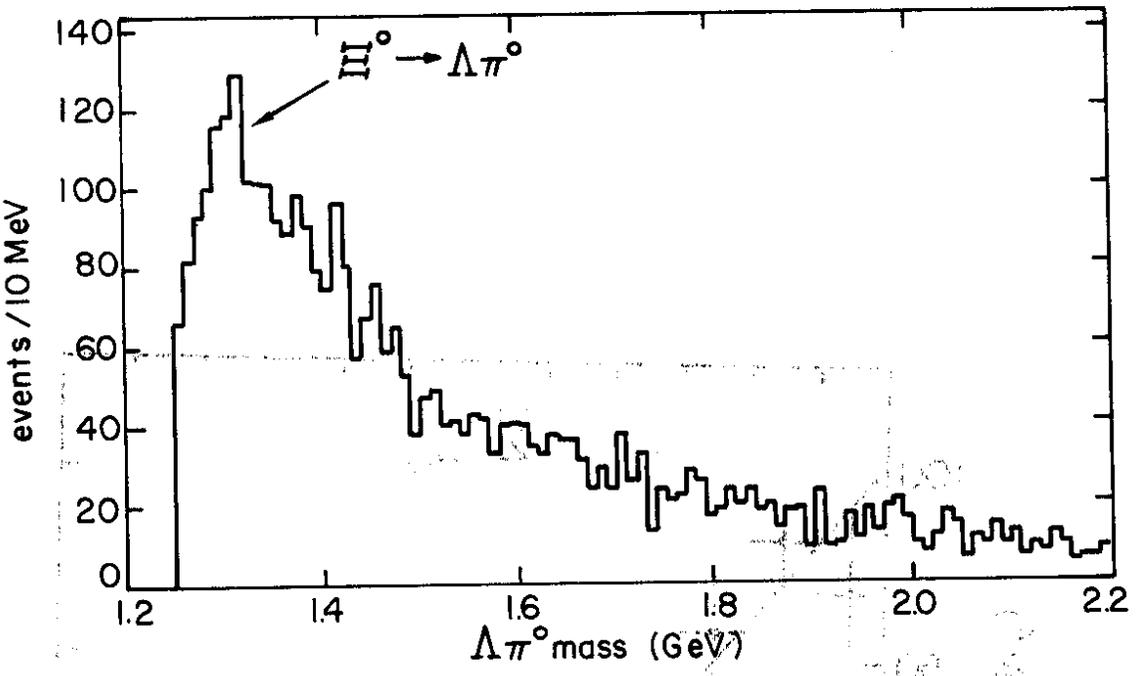

Fig. 10 (a)

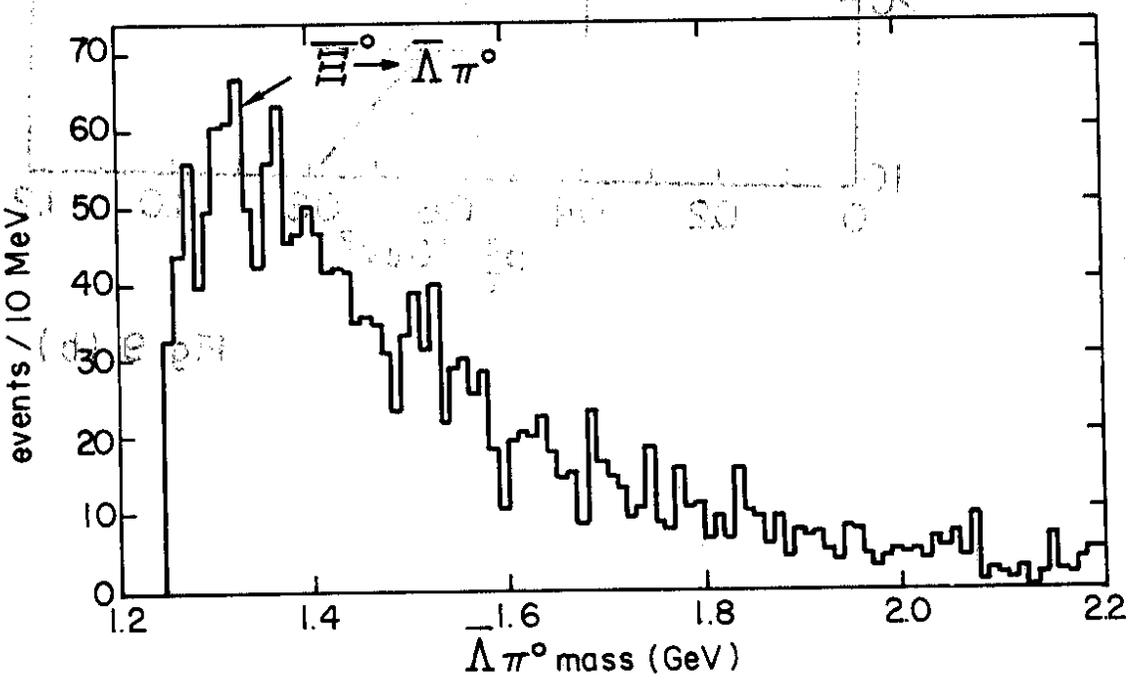

Fig. 10 (b)

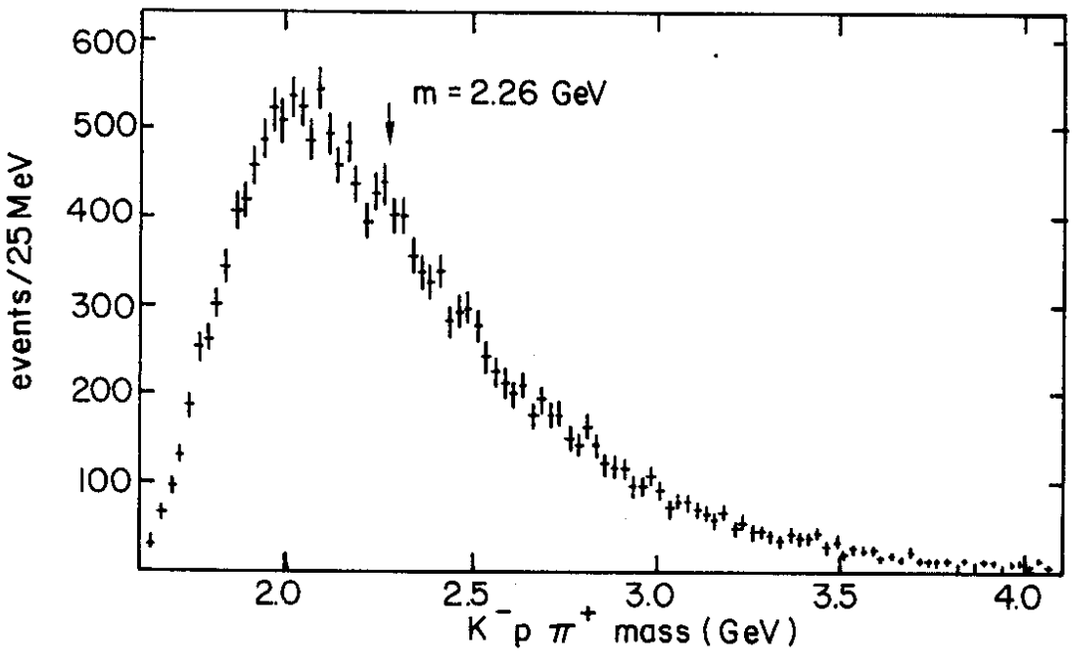

Fig. 11 (a)

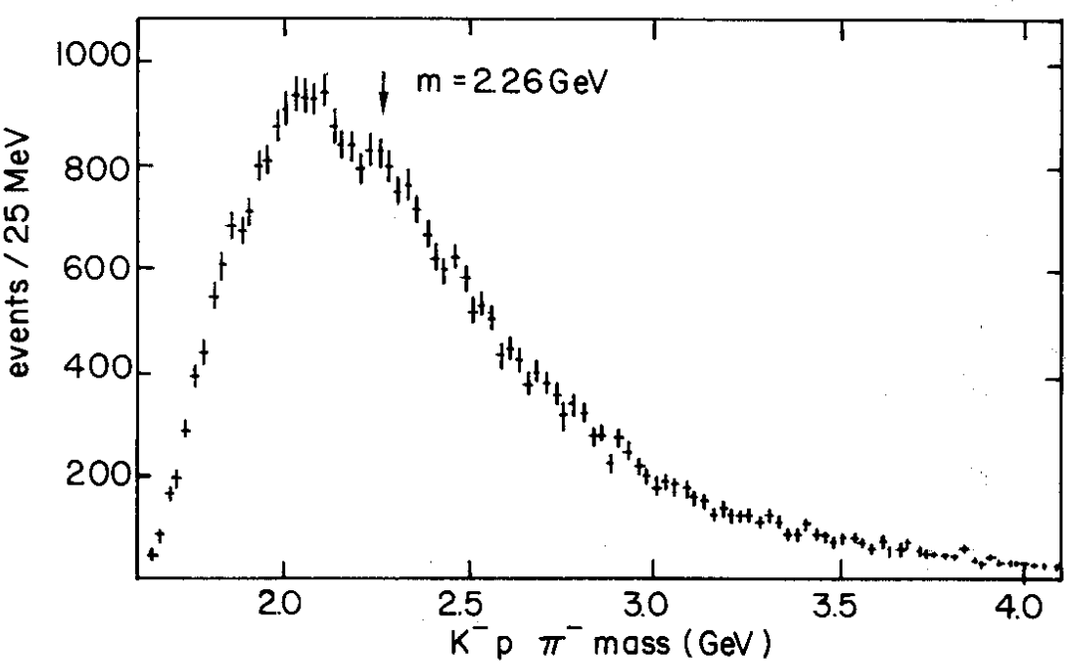

Fig. 11 (b)

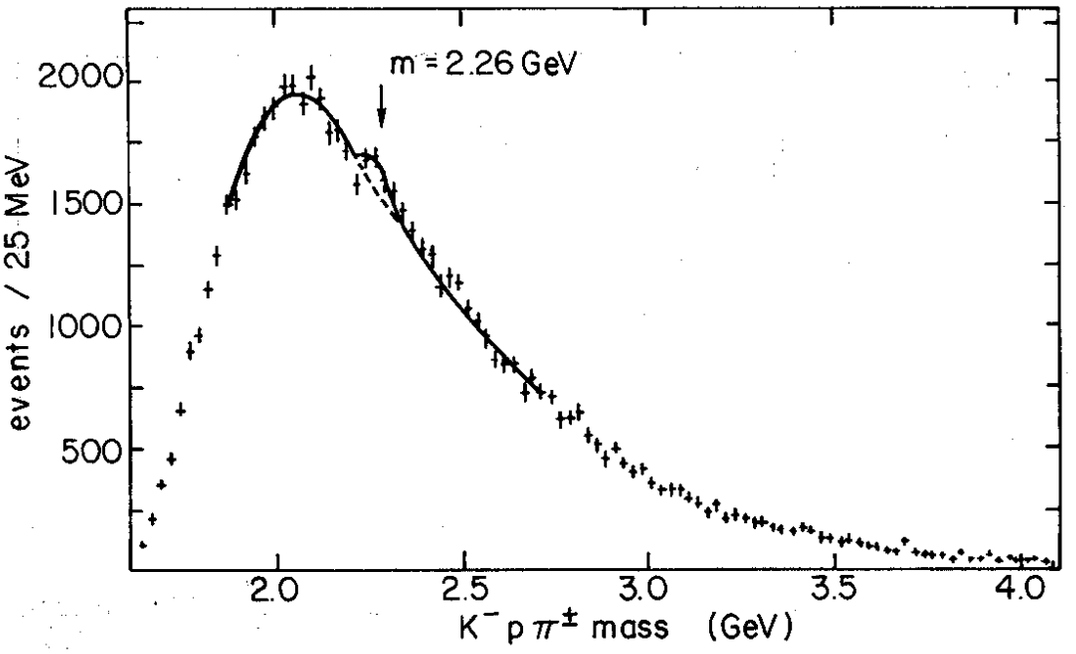

Fig. 11 (c)

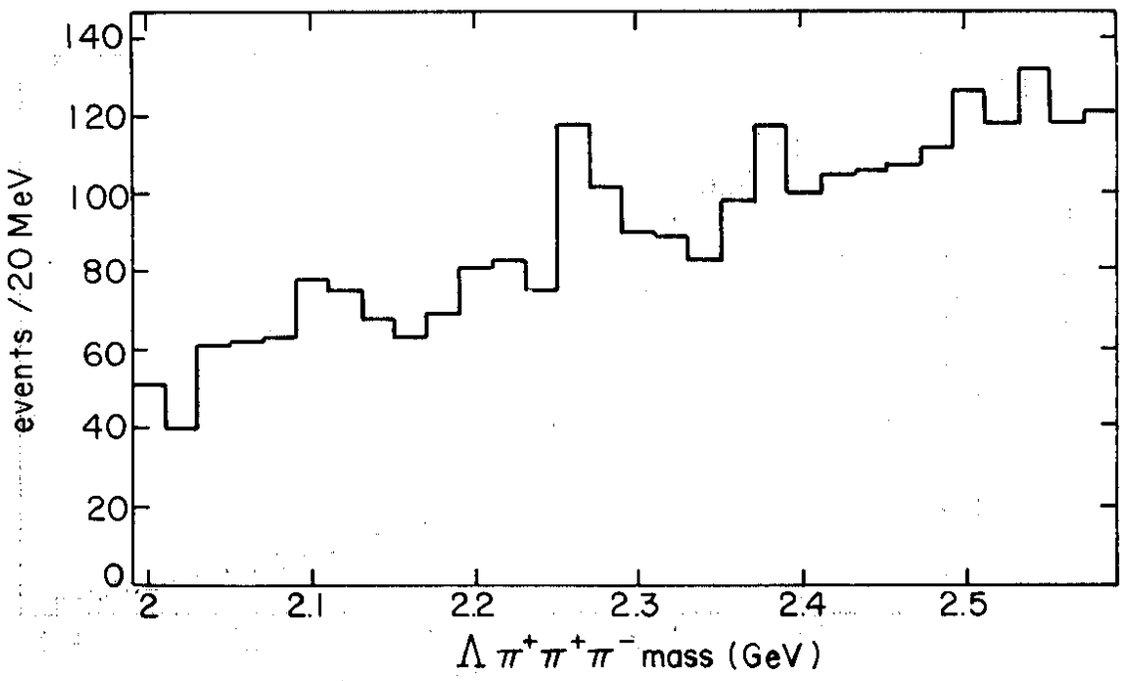

Fig. 11(d)

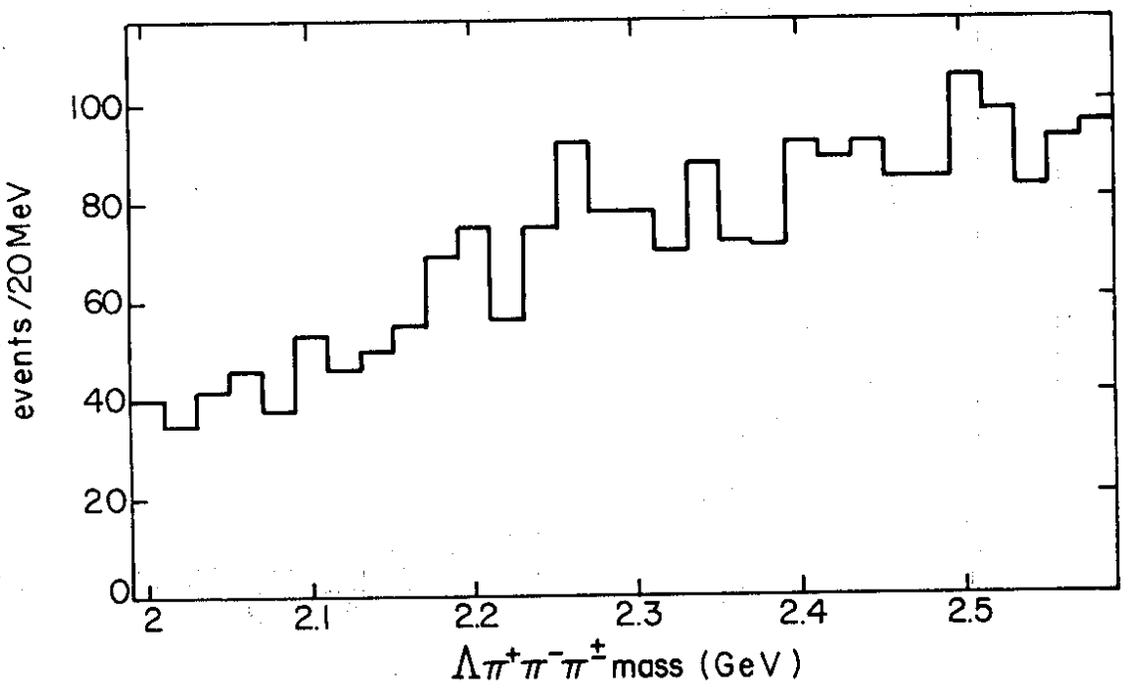

Fig. II (e)

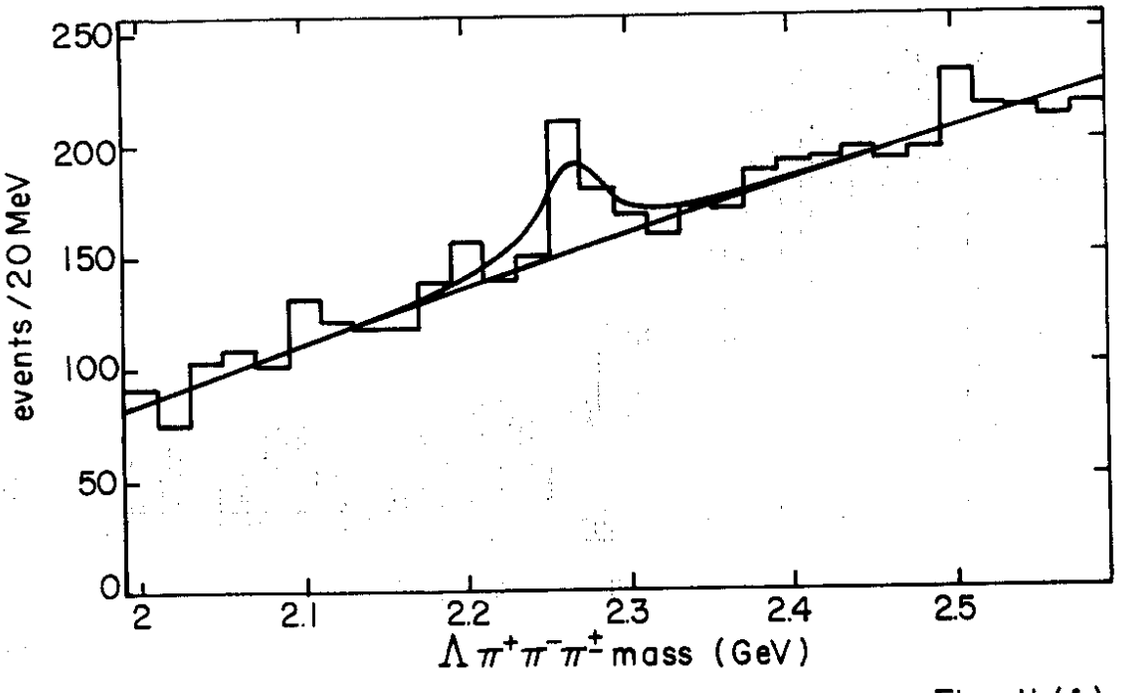

Fig. II (f)

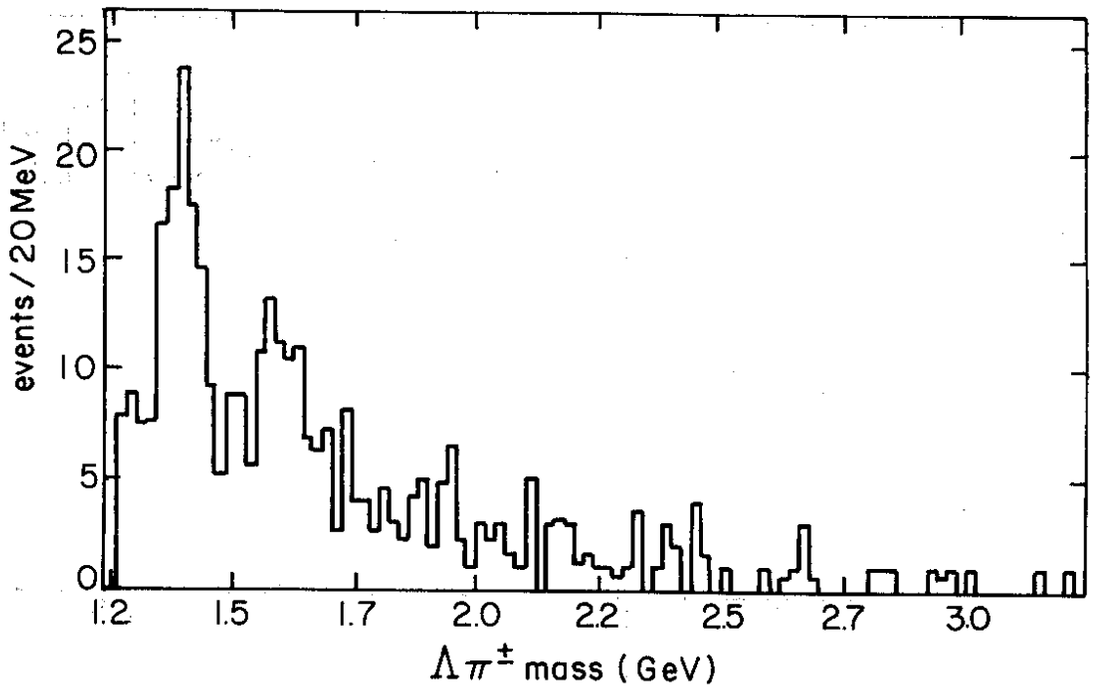

Fig. 12(a)

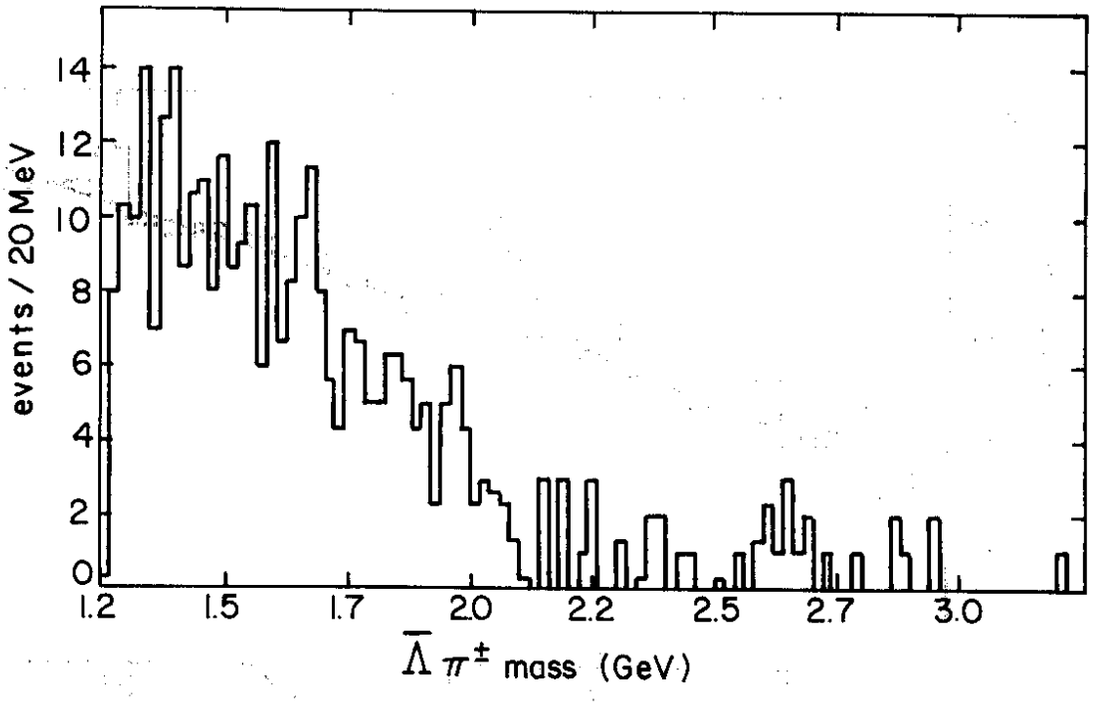

Fig. 12(b)

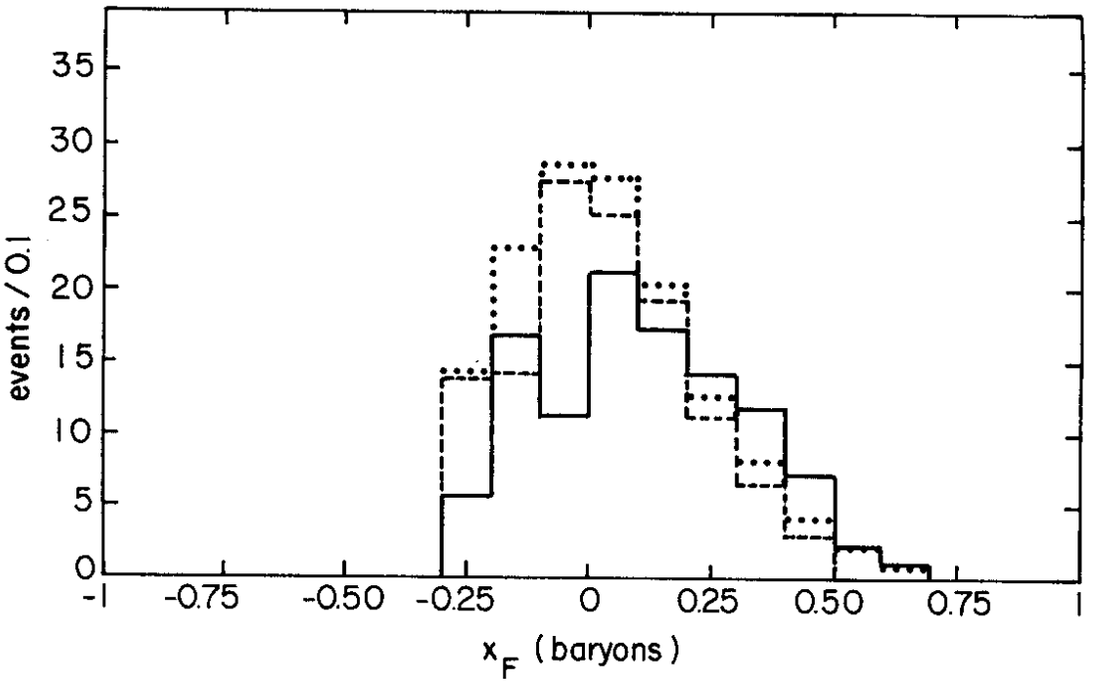

Fig. 13(a)

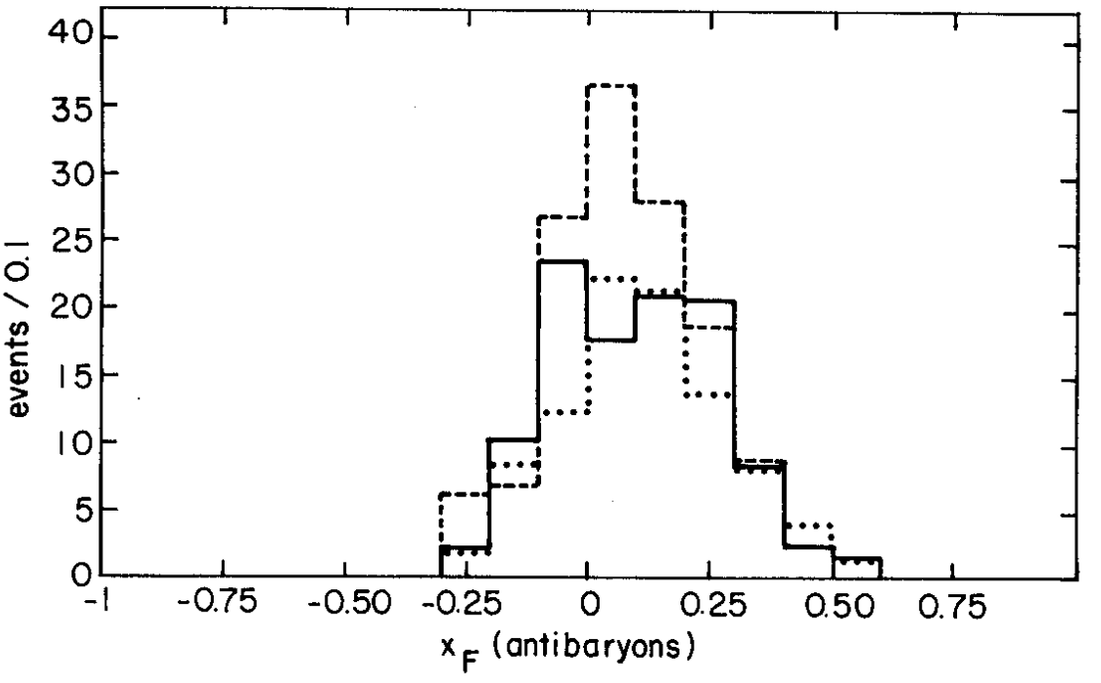

Fig. 13(b)